Unitary IPSPs enhance hilar mossy cell gain in the rat hippocampus

Angharad M. Kerr and Marco Capogna

MRC, Anatomical Neuropharmacology Unit, Mansfield Road, OX1 3TH Oxford, UK

Mechanisms that control neuronal gain allow for adaptive rescaling to synaptic inputs of varying strengths or frequencies. Here, we show that unitary IPSPs (uIPSPs) modulate gain and unitary EPSP (uEPSP)-action potential coupling in mossy cells (MCs) from rat hippocampal slices. Mossy fibre-evoked uEPSCs were large, facilitated and were suppressed by the group II metabotropic glutamate agonist LY354740. Conversely, uIPSCs were smaller, depressed and were not affected by LY354740, but exerted strong inhibitory control over uEPSP-action potential coupling. The IPSC reversal potential was determined by gramicidin perforated patch recordings to be -65.3 ± 5.0 mV, lying between the resting membrane potential (-75.3 ± 1.1 mV) and the action potential threshold (-56.5 ± 2.4 mV). When applied at theta frequency (10 Hz), uIPSPs increased the offset of the MC input–output response to depolarizing current injection, but also increased gain, maximal firing rate and the slope of the depolarization preceding action potentials. These effects were unchanged by the Ca^{2+} and HCN channel blockers mibefradil and ZD7288, respectively. The height and maximal slope of MC action potentials during tonic depolarization were also increased by uIPSPs, and the decay of uIPSP conductances injected by dynamic clamp at subthreshold membrane potentials was prolonged by TTX. Application of the muscarinic agonist pilocarpine mimicked the effect of IPSPs on MC maximal firing rate, and action potential height and slope, and this was reversed by the $GABA_A$ antagonist gabazine. Thus, uIPSPs can increase neuronal gain under hyperexcitable conditions, and this effect is probably due to the de-inactivation of a TTX-sensitive voltage-dependent Na^+ conductance.

(Resubmitted 21 September 2006; accepted 25 October 2006; first published online 2 November 2006)
Corresponding author M. Capogna: MRC, Anatomical Neuropharmacology Unit, Mansfield Road, OX1 3TH Oxford, UK. Email: marco.capogna@pharm.ox.ac.uk

Neuronal information processing determines the relationship between the inputs a cell receives and the output it generates as a response. This input–output (I–O) relationship displays two main characteristics: the offset, or the amount of input required to generate any output, and the gain, or the response/sensitivity of the neuron to a given change in its input. Most studies have demonstrated that a fixed tonic inhibitory shunting conductance induces a shift in the offset of the *I–O* relationship of a neuron to excitatory tonic current injection, with little effect on neuronal gain (Granit *et al.* 1966; Berman *et al.* 1992; Holt & Koch, 1997). However, both tonic and synaptic-like or phasic shunting inhibition can, in fact, substantially depress neuronal gain in the presence of phasic excitation (Mitchell & Silver, 2003).

GABAergic synaptic inputs cooperate with excitatory inputs to determine the dynamic control of cell output, and modulate the efficacy and reliability of an excitatory synapse by many means. IPSPs mediate hyperpolarization and/or shunting inhibition, which can silence neuronal firing (Coombs *et al.* 1955; Tamas & Szabadics, 2004). Alternatively, GABAergic transmission can depolarize neurons and enhance firing (Gulledge & Stuart, 2003; Marty & Llano, 2005). Interestingly, GABAergic transmission has also been observed to entrain neuronal firing (Lytton & Sejnowski, 1991; Cobb *et al.* 1995; Bartos *et al.* 2001; Gulledge & Stuart, 2003; Bacci & Huguenard, 2006), and shape the time window for spike generation and coincidence detection (Pouille & Scanziani, 2001, 2004).

Integration of EPSPs and IPSPs can also be influenced by intrinsic membrane conductances. In accordance, spike time reliability is maximal for those stimuli that contain frequencies matching the neuronal intrinsic frequency of firing (Hunter *et al.* 1998). Furthermore, the activation of Na^+ conductances at subthreshold voltages has been observed to either boost or actively terminate IPSPs (Stuart, 1999; Baufreton *et al.* 2005, respectively) and facilitate EPSP–spike coupling (Fricker & Miles, 2000),

DOI: 10.1113/jphysiol.2006.121608

whereas dendritic hyperpolarization-activated cation channels (HCN) enhance the attenuation of depolarizing IPSPs (Williams & Stuart, 2003).

Hilar mossy cells (MCs) are glutamatergic neurons and an integral component of the hippocampal dentate gyrus–CA3 network (Amaral, 1978; Buckmaster & Schwartzkroin, 1994; Ratzliff *et al.* 2002). MCs integrate convergent excitatory and inhibitory inputs, and then return this information to granule cells in a recurrent positive feedback circuit (Ribak *et al.* 1985; Frotscher *et al.* 1991; Soriano & Frotscher, 1994; Wenzel *et al.* 1997; Lisman, 1999). MCs constitute a highly excitable cell type and are likely to play important roles in temporal lobe epilepsy and learning/memory processes (Buckmaster & Schwartzkroin, 1994; Lisman, 1999; Lysetskiy *et al.* 2005). Although a wealth of data on MCs are available (Scharfman & Schwartzkroin, 1988; Scharfman *et al.* 1990; Buckmaster *et al.* 1993; Soltesz *et al.* 1993; Scharfman, 1994, 1995; Frazier *et al.* 2003; Jinno *et al.* 2003; Ratzliff *et al.* 2004; Lysetskiy *et al.* 2005), it is not yet understood how they integrate their diverse synaptic inputs. Thus, MC function remains controversial and their computational properties are little known.

Here we study the synaptic integration of unitary EPSCs (uEPSCs) and unitary IPSCs (uIPSCs) in MCs, providing novel insights on the function of MCs in normal conditions and during hyperexcitability, and also showing how excitatory and inhibitory synapses can cooperate to dynamically control neuronal output.

Methods

Preparation of acute slices

All procedures involving animals were performed according to methods approved by the UK Home Office and The Animals (Scientific Procedures) Act, 1986. Every effort was made to minimize the number of animals used and their suffering. Acute horizontal slices were prepared from 14- to 23-day-old-male Sprague-Dawley rats (Charles River, Margate, UK). Rats were deeply anaesthetized with isoflurane in oxygenated air and then decapitated. The brain was rapidly removed and placed in semifrozen sucrose ACSF cutting solution containing (mM) 75 sucrose, 87 NaCl, 2.5 KCl, 0.5 $CaCl_2$, 7 $MgCl_2$, 1.25 NaH_2PO_4, 25 $NaHCO_3$, 25 glucose, pH 7.3 and bubbled with 95%O_2, 5%CO_2. Horizontal slices (350 μm) were cut from the middle to the ventral portion of the hippocampus (Leica VT 1000S, Leica Microsystems GmbH, Nussloch, Germany) and transferred to a nylon mesh where they were maintained in a chamber containing sucrose ACSF at 37°C for 30 min before returning to room temperature (24–26°C) for another 30 min. During this 1 h time period, sucrose ACSF was substituted with normal ACSF (for constituent components, see below) at a rate of 1–2 ml min^{-1}.

Electrophysiology

Acute slices were secured under a nylon mesh and submerged and superfused (at 1–2 ml min^{-1} and at 34°C) with ACSF, containing (mM) 130 NaCl, 3.5 KCl, 2.5 $CaCl_2$, 1.5 $MgSO_4$, 1.25 NaH_2PO_4, 24 $NaHCO_3$, 10 glucose (all from VWR International, Lutterworth, UK), pH 7.4 (bubbled with 95%O_2, 5%CO_2), in a 2 ml chamber mounted on the stage of an upright microscope (Axioskop, Zeiss, Jena, Germany). Slices were visualized with a 40× water-immersion objective (Zeiss, Oberkochen, Germany) coupled with infrared and differential interference contrast (DIC) optics linked to a video camera (Newvicon C2400, Hamamatsu, Hamamatsu City, Japan). Somatic whole-cell patch-clamp recordings (33–35°C) were made from visually identified cells using borosilicate glass capillaries (GC120F, 1.2 mm o.d., Clarke Electromedical Instruments, Reading, UK, 3–6 MΩ), pulled on a DMZ puller (Zeitz-instrumente GmbH, Munich, Germany) and filled with a filtered intracellular solution consisting of (mM): 126 K-gluconate, 4 KCl, 4 ATP-Mg, 0.3 GTP-Na_2, 10 Na_2-phosphocreatine, 10 Hepes and 0.5% w/v biocytin (all from Sigma-Aldrich Co. Ltd, Poole, UK), osmolarity 270–280 mosmol l^{-1} without biocytin, pH 7.3 with KOH. Biocytin was added to allow *post hoc* visualization of the recorded neurons. Cells were only accepted if the initial seal resistance was greater than 1 GΩ. *I–V* protocols were performed in current-clamp mode to assess the firing pattern of recorded cells in response to depolarizing rectangular current pulses, and input resistance (R_{in}) was calculated offline from the slope of a line fitted to the subthreshold range on a plot of the injected current *versus* the steady-state membrane voltage when a family of hyperpolarizing and depolarizing current injections were applied (range, −30 pA to 165 pA). The series resistance (R_s) was compensated online by 60–70% in voltage-clamp mode to reduce voltage errors, and cells were only accepted for analysis if the initial R_s was less than or equal to 25 MΩ (range, 14–25 MΩ) and did not change by more than 20% throughout the recording period. Throughout the text and figures, membrane potentials for all whole-cell recordings have been corrected for an experimentally determined liquid junction potential of −12 mV. All electrophysiological signals were amplified (10 mV pA^{-1}, EPC9/2 amplifier HEKA Electronik, Lambrecht, Germany, PULSE software), filtered at 2.9 kHz, digitized at 5 or 10 kHz, and the amplifier was controlled from a personal computer (Power Mac G4, Macintosh or Systemax PC, AMD Athlon Processor, Systemax Systems) running the PULSE data acquisition and analysis programme (HEKA). Currents/voltages were acquired online with

Pulse software (HEKA, see above) and analysed offline with Pulsefit (HEKA) and IGOR (Wavemetrics Inc, Oregon, USA). The apparent membrane time constant (τ) was calculated with IGOR software by fitting a single exponential to the response of the cell to a current injection of −30 pA in current-clamp mode. The sag ratio was calculated from the membrane potential at the end of a 1 s hyperpolarizing pulse divided by the largest membrane potential change observed in response to a current step of −100 pA. Membrane capacitance was calculated as τ/R_{in}. Action potentials were elicited by application of a depolarizing current step (5 ms, 800 pA), and action potential half-width was calculated by a user-defined programme in IGOR.

Extracellular stimulation was conducted by applying rectangular pulses of current (0.4 ms width, intensity range: 8.5–45 μA) delivered through an isolation unit (A360 Stimulus Isolator, World Precision Instruments, Stevenage, UK) to a monopolar patch pipette filled with ACSF. The monopolar stimulating electrode was placed within the granule cell layer, to generate IPSCs, or at the border of the granule cell layer and the hilus, to generate EPSCs.

Evoked synaptic events were measured using Pulsefit software. The latency of unitary events was determined as the time between the positive peak amplitude of the stimulation artefact and the onset of the postsynaptic response, which was defined as the point at which the amplitude could be visualized to deviate from background noise level. A failure was defined as a trial in which no event could be visually detected, and the failure rate was calculated as the number of failures divided by the number of trials. The unitary event peak amplitude was visually delimited and then measured using Pulsefit. One or more files of 30 or 50 trials were analysed for each unitary response. Latency and amplitude values (failures not included) were averaged for the trials, and the jitter of the response was defined as the standard deviation of the latency. Sometimes a paired-pulse protocol was used, whereby two stimuli were evoked with a 25 ms interval. The paired-pulse ratio was calculated as the mean peak amplitude of the response to the second stimulus divided by the mean peak amplitude of the response to the first stimulus. Traces were averaged for each file and the decay phase was fitted with a single exponential to give the decay τ for the synaptic response. The 20–80% rise time was calculated with a user-defined programme in IGOR.

Steps of tonic, depolarizing current were injected into MCs in whole-cell patch clamp (range 5–300 pA, 6 s). The mean frequency of action potentials was calculated for the whole duration of current application and plotted against the injected current amplitude. The data were fitted by the following equations, as in Mitchell & Silver (2003). To calculate for the gain and offset of the *I–O* relationship in control conditions, eqn (1) was applied:

$$f(x) = k\ln(x) - A \quad (1)$$

where f = firing frequency (Hz); x = injected tonic current step (pA); k = gain or slope of *I–O* curve (Hz pA^{-1}); $\exp(A/k) = x$-offset (pA); $A = k\ln(x\text{-offset})$ (Hz).

Subsequently, the following eqn (2) was used to fit data from *I–O* curves in the presence of inhibition, while constraining k and A parameters to the values calculated from eqn (1):

$$f(x) = m(k\ln(x - C) - A) \quad (2)$$

where m = change in gain or slope of *I–O* curve; C = shift in offset due to inhibition (pA).

The slope of the subthreshold voltage trajectory before an action potential, or the 'prepotential', was analysed by fitting a straight line between the start and end of the prepotential and averaging this slope for the first five action potentials after 1 s of the 160 pA depolarizing current step. The height of the action potential evoked by depolarizing current pulses was analysed by averaging the peak amplitude of the first five action potentials after 1 s of a depolarizing current step (151 ± 13 pA, $n = 7$) from the threshold potential. The height of the action potential evoked by pilocarpine or pilocarpine and gabazine was calculated from the threshold to the peak of each action potential occurring in an epoch of 120 s for each experimental condition. Likewise, the inter-event intervals between action potentials were calculated in epochs of 250 s for each experimental condition, by using MiniAnalysis (Synaptosoft, Decatur, GA, USA). Power spectral analysis was performed after fast Fourier transformation (FFT) on low-pass-filtered signals (<5 kHz) in epochs of 250 s of recording. The resting membrane potential during pilocarpine and pilocarpine and gabazine applications was calculated during the interspike intervals. The maximal slope of the action potentials was calculated by averaging the maximal amplitude of the differentiated traces containing the first five action potentials after 1 s of depolarizing current steps (151 ± 13 pA, $n = 7$). The maximal slope for each action potential evoked by pilocarpine with or without gabazine was calculated by the maximal amplitude of the differentiated trace for each action potential, and these values were averaged in epochs of 2 min for each experimental condition.

Synthetic (dynamic clamp) IPSPs (dIPSPs) or EPSPs (dEPSPs) were applied through the patch pipette using a synaptic module (SM-1) conductance injection amplifier (Cambridge Conductance, Cambridge, UK). The dynamic conductance waveform for an IPSP was based on the magnitude, kinetics and reversal potential of the IPSC experimentally evoked by minimal stimulation in the same cell in voltage

clamp prior to the dynamic-clamp experiment (range: peak conductance = 2.58–3.75 nS, 20–80% rise time = 0.49–0.61 ms, decay τ = 5.65–6.22 ms, experimentally observed reversal potential = −86 to −92 mV). The dynamic conductance waveform for an EPSP was also based on the EPSC evoked by minimal stimulation in the same cell in voltage clamp prior to the dynamic-clamp experiment (range: peak conductance = 2.04–3.65 nS, 20–80% rise time = 0.43–0.49 ms, decay τ = 3.73–4.16 ms, reversal potential set at 0 mV).

Perforated-patch recordings were conducted with pipettes with a resistance of 2.5–5 MΩ and back-filled with an internal solution containing (mM): 78KCl, 78 K-gluconate, 5 $MgCl_2$, 10 Hepes, 5 glucose, 15–20 μg ml^{-1} gramicidin-D (Sigma) and 0.05 Alexa 594 (Invitrogen GmbH, Kahlsruhe, Germany), pH 7.3 with KOH, 315 mosmol l^{-1}. To ease seal formation, the tip of the pipette was filled with the same solution omitting gramicidin-D. Recordings were made between 23°C and 25°C and under visual control from MCs with their soma in the hilus. As spontaneous passage to whole-cell configuration was frequently observed, recorded cells were visualized with epifluorescence illumination for short intervals, to ensure the integrity of the perforated patch configuration throughout the recording period, and fluorescent labelling of the cell, accompanied by depolarization of the GABA reversal potential (E_{GABA}), indicated a rupture of the perforated configuration. Furthermore, the seal was monitored throughout experiments by application of a 5 mV pulse, and experiments were started when the R_s was less than 150 MΩ (93.87 ± 17.73 MΩ, n = 5). Currents were acquired with an Axopatch 200A amplifier, low-pass filtered at 5 kHz and digitized at 20 kHz with a CED1401plus laboratory interface connected to a personal computer. Stimulus generation, data acquisition and analysis were carried out using homemade procedures in IGOR (FPulse/FEval, made in the laboratory of Professor Jonas, Freiburg, Germany). IPSCs were elicited with rectangular pulses of voltage (0.2–0.4 ms width, intensity range: 9–48 V) applied at a frequency of 0.25 Hz and delivered through a constant-voltage source (made in the laboratory of Professor Jonas) to a monopolar patch pipette filled with ACSF. Stimulating electrodes were placed within the granule cell layer and IPSCs were isolated by application of 6-cyano-7-nitroquinoxaline-2,3-dione (CNQX), DL-2-amino-5-phosphonovaleric acid (AP5) and CGP55845A. Holding potentials were set to values between −100 mV and −20 mV, and R_s was compensated 40–70%, lag 35 μs. Evoked IPSC amplitudes were measured as the peak current minus the baseline, and averaged from 20 traces for each holding potential. The resulting I–V relationships were fitted with a second-order polynomial function to determine the E_{GABA}, which was corrected for an experimentally determined liquid junction potential of −6 mV.

Histological processing of recorded cells

After electrophysiological recordings, slices were sandwiched between two filter papers (cellulose nitrate membrane filters, 0.45 μm, Whatman International Ltd, Maidstone, UK) and immersed in a fixative of 4% paraformaldehyde and 15% saturated picric acid in phosphate buffer (PB, 0.1 M, pH 7.4) for at least 24 h. Then, slices were embedded in a block of gelatin and re-sectioned into 50–60 μm slices with a Leica VT 1000S vibroslicer. Sections were washed in Tris-buffered saline (TBS; 0.9% NaCl, 0.05 M Tris, pH 7.4) and incubated overnight at 4°C in a 1 : 100 solution of avidin-biotinylated horseradish peroxidase complex (Vector labs, Burlingame, CA, USA) in TBS + 0.1% Triton X-100 (VWR International). Sections were further washed in TBS and Tris buffer (TB, 0.05 M, pH 7.4) before incubation in 0.5 mg ml^{-1} diaminobenzidine (DAB, Sigma) in TB. Hydrogen peroxide (0.01%) was the substrate for the peroxidase reaction, which was carried out in TB. Sections were rinsed in TB, then PB and subsequently mounted on gelatine-coated slides and left to air dry overnight. Slides were incubated in a solution of 0.08% osmium tetroxide, washed in PB, dehydrated in graded ethanol (EtOH; 50%, 70%, 90%, 95% and 100% × 2), immersed in xylene and permanently mounted on slides. Neurons were reconstructed using a drawing tube. A 40× objective was used to draw the cells.

Statistical tests

Data throughout the text are presented as mean ± S.E.M. Where the number of observations for a given experiment was >7, a homogeneity of variance test was applied to determine if the variances of the groups were different, and where they were the same, a parametric test was used to determine the significance level for the data. Where the groups had significantly different variances or when the number of observations was = 7, a non-parametric test was applied. The mean values for P(success) and latency from the experiments to determine the action of uIPSPs on uEPSP–action potential coupling were compared with a one-way analysis of variance (ANOVA) test on the non-normalized data, combined with a Bonferroni *post hoc* comparison. Mean jitter, however, was compared with a Kruskal–Wallis test and compared with Dunn's procedure for non-parametric multiple group comparisons for groups with unequal n values, since the variance of the groups was significantly different for this set of data. A Wilkoxon signed ranks test was generally applied to compare two groups of data unless the data were from

two independent samples, when a Mann–Whitney test or *t* test for independent samples was used.

Chemicals and drugs

All drugs were superfused to the slices through the bath solution. Salts used for the patch pipette solution and ACSF were obtained from either VWR International or Sigma. Drugs, unless otherwise stated (Tocris Cookson Inc, Avonmouth, UK) were added at the following concentrations: CNQX, 20 μM; LY354740, 0.5 μM; gabazine, 1.2 μM or 10 μM, 6,7-dinitroquinoxaline-2,3-dione (DNQX), 20 μM; AP5, 40 μM; ZD7288, 30 μM; mibefradil, 1–5 μM; tetrodotoxin (TTX), 1 μM; pilocarpine, 0.5 mM; atropine, 50 μM; CGP55845A, 5 μM.

Results

Anatomical and physiological features of recorded MCs *in vitro*

MCs were putatively identified online by their somatodendritic features and electrophysiological responses. In particular, MCs have a large membrane capacitance and apparent membrane time constant, and display a small sag in response to hyperpolarizing current injection (Fig. 1*B*, Table 1). Care was taken to avoid cells

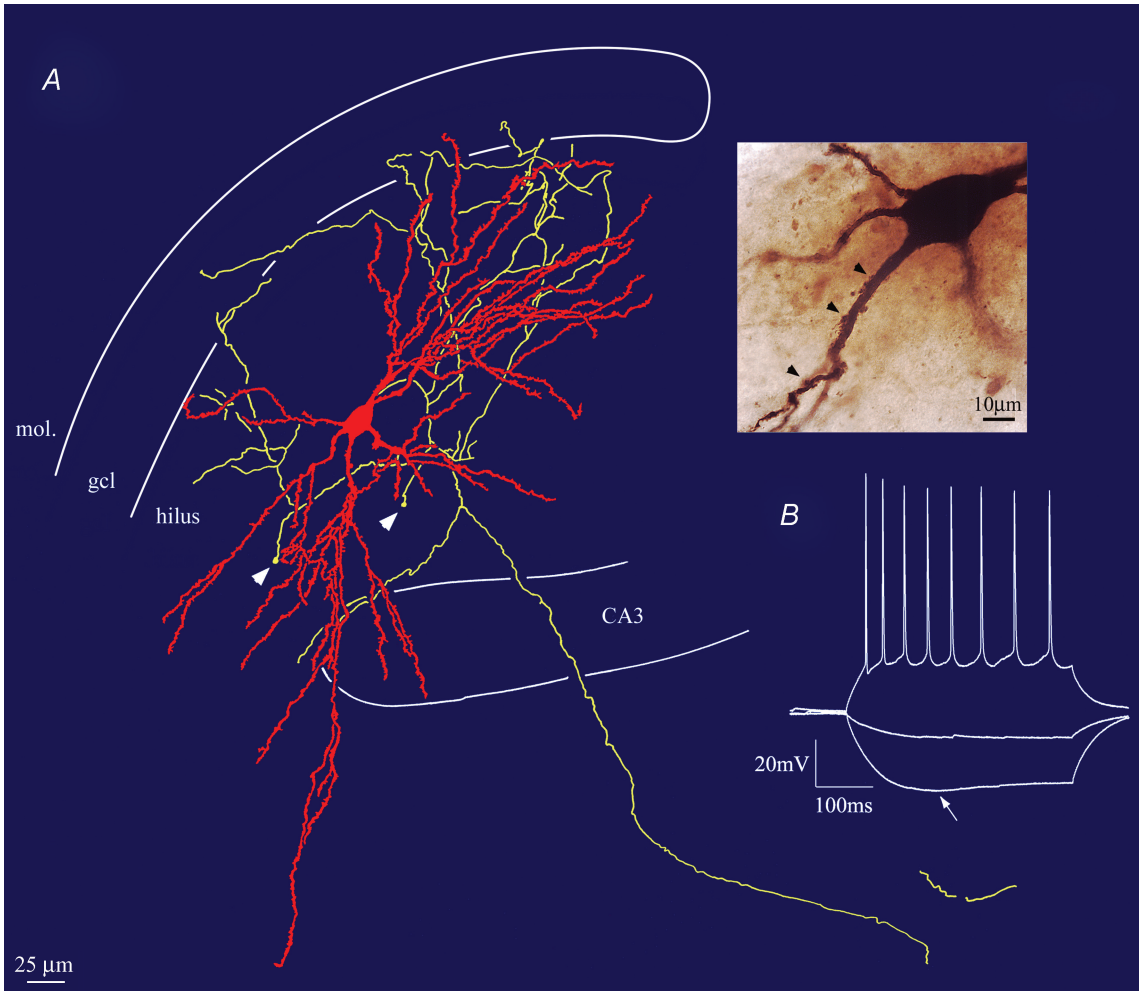

Figure 1. Features of hilar MCs in acute slices
A, drawing tube reconstruction of biocytin-filled MC soma and processes. Thick red lines represent dendrites, whereas the axon is indicated in yellow. Solid white lines demarcate cell layers and arrowheads point to axons that have been cut by the slice preparation, mol., molecular cell layer, gcl, granule cell layer. Upper insert contains a light micrograph of MC soma and proximal dendrites (arrowheads highlight complex spines, or thorny excrescences, on the proximal dendrites). *B*, the traces show the typical response of a MC to depolarizing and hyperpolarizing current injection. Arrow points to a small sag, presumably mediated by HCN channels.

Table 1. Mossy cell intrinsic membrane properties and recording parameters

Age (days)	Rmp (mV)	Membrane capacitance (pF)	Membrane τ (ms)	Input resistance (MΩ)	Sag ratio	Action potential half width (ms)	Series resistance (MΩ)
19 ± 0.4 (34)	−75.3 ± 1.1 (32)	207.6 ± 9.5 (33)	52.3 ± 12.8 (31)	244.9 ± 13.8 (32)	0.91 ± 0.01 (27)	0.93 ± 0.04 (21)	18.1 ± 0.7 (34)

Values quoted represent mean ± S.E.M. for *n* cells, Rmp, resting membrane potential.

near the CA3 region, as it is otherwise possible that displaced CA3 pyramids can be mistaken for MCs. Patch electrodes contained biocytin, and all recorded cells were processed to reveal their anatomical characteristics; 92% of recorded cells were recovered and positively identified as MCs by their characteristic anatomical features, namely the presence of complex spines on proximal dendrites and their axonal and dendritic arborization. Only recordings from anatomically identified MCs were included in the study. MC somata and much of their dendritic arbour were located in the hilus (Fig. 1*A*). Much of the axon appeared to be cut in the slice preparation (see arrowheads in Fig. 1*A*), but otherwise extended into the granule and molecular cell layers, with a major component projecting towards the fimbria.

uIPSCs and mossy fibre-meditated uEPSCs recorded in MCs

Putative mossy fibre-mediated uEPSCs were evoked by minimal stimulation of excitatory fibres at the border between the granule cell layer and the hilus in the presence of the $GABA_A$ receptor antagonist gabazine (1.2 μM). Initially, the stimulation intensity was moderate (50–100 μA), to aid in the detection of connected fibres. Then, when an EPSC was observed, the stimulation intensity was reduced so that failures always appeared. The stimulation intensity and position of the stimulating electrode were then adjusted such that a response appeared, but was abolished if the stimulation intensity was turned down by a small amount. Responses were accepted as unitary if the amplitude remained constant over a range where failures dropped, and the stimulation intensity chosen corresponded to the value that gave the least amount of failures within this amplitude range (Fig. 2*Aa* and *Ab*). uEPSCs were characterized by a large amplitude, fast rise times and fast decay times (Table 2 and Fig. 2*Aa*). A facilitating/depressing pattern was observed when a 40 Hz train was applied (Fig. 2*Ac*). Paired-pulse facilitation was observed under control conditions, and this was enhanced by application of the group II mGluR agonist LY354740 (0.5 μM), suggesting that uEPSCs were mediated by stimulation of a single mossy fibre (Kamiya *et al.* 1996). Furthermore, LY354740 dramatically increased the number of failures (Fig. 2*Ad*). Quantitatively, LY354740 reduced the uEPSC peak amplitude to 27 ± 3% of control, enhanced the paired pulse ratio to 420 ± 45% of control and enhanced failures from 2 ± 1% to 62 ± 9% of trials ($n = 3$).

Minimal stimulation of inhibitory fibres in the granule cell layer evoked uIPSCs in the presence of DNQX (20 μM) and AP5 (40 μM). The initial process was identical to that outlined above for uEPSCs, apart from the application of one additional criterion: the uIPSC had to be close to all-or-none, with little variation in amplitude (Fig. 2*Ba* and *Bb*). The uIPSCs had moderate amplitude, low probability of failure, fast rise times and depressed at 40 Hz stimulation (Table 2, Fig. 2*Ba* and *Bc*). Unlike uEPSCs, uIPSCs were unaffected by the application of 0.5 μM LY354740 (Fig. 2*Bd*, peak amplitude 100 ± 3% of control, paired pulse ratio 99 ± 4% of control, $n = 3$). To summarize, MCs are subject to powerful unitary excitatory and inhibitory synaptic influences. Despite the much larger amplitudes of uEPSCs as compared to uIPSCs at $V_h = -60$ mV, the peak conductance generated by the two events was comparable (Table 2). Both PSCs displayed short latencies and jitter, consistent with a monosynaptic response.

In order to better understand the physiological impact of $GABA_A$-mediated inhibitory currents on membrane potentials, we investigated the reversal potential for IPSCs (E_{GABA}) under conditions where the intracellular chloride concentration remained unperturbed, namely with gramicidin-D perforated-patch recordings. IPSCs were stimulated with an extracellular electrode in the granule cell layer, pharmacologically isolated and evoked while holding the MC at potentials between −100 mV and −20 mV (Fig. 3*B*). The mean E_{GABA} for five recorded MCs was −65.3 ± 5.0 mV (Fig. 3*C*). This was significantly more positive than the resting membrane potential, −75.3 ± 1.1 mV ($P < 0.05$, Mann–Whitney test), as determined with whole-cell recordings (Table 1).

Next, we wished to address how uIPSCs influence the output of MCs. Are these unitary inputs capable of modulating the large amplitude mossy fibre-mediated uEPSCs, and changing EPSP-action potential coupling?

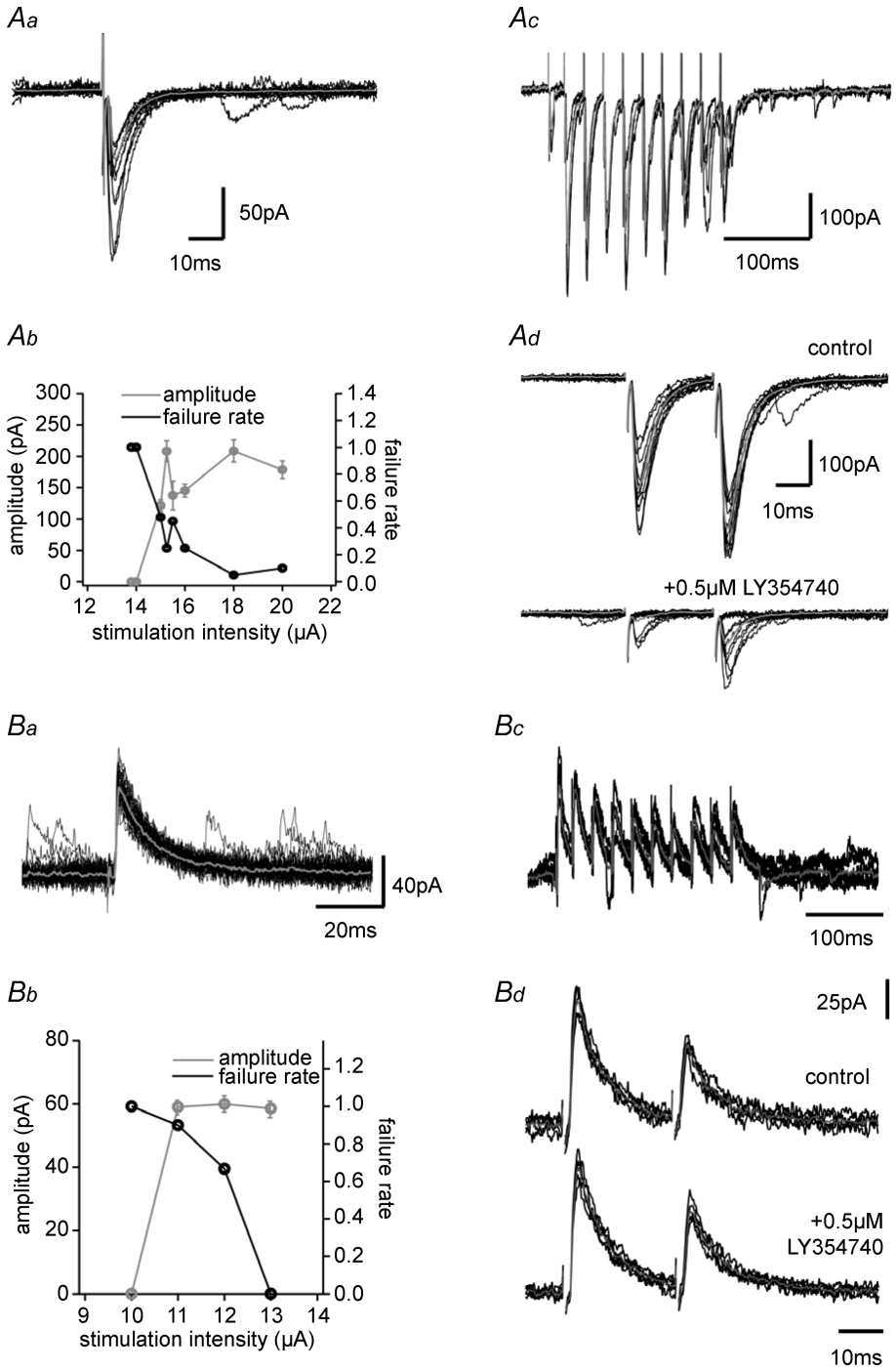

Figure 2. Minimal stimulation of mossy fibre inputs at the granule cell–hilus border and inhibitory fibres in the granule cell layer

Aa, example traces (black line) and average (thick grey line) of uEPSC responses to stimulation of mossy fibres. *Ab*, plot of uEPSC amplitude and failure rate *versus* stimulation intensity. *Ac*, response of mossy cell to 40 Hz stimulation of mossy fibres. *Ad*, paired-pulse facilitation was observed in control conditions. Addition of LY354740 (0.5 μM) increased the number of failures, decreased uEPSC amplitudes and increased the paired-pulse ratio. All recordings were carried out in the presence of 1.2 μM gabazine at a holding potential (V_h) = −72 mV. *Ba*, example traces (black line) and average (thick grey line) of uIPSC responses to minimal stimulation of inhibitory fibres. *Bb*, plot of uIPSC amplitude and failure rate *versus* stimulation intensity. *Bc*, response of mossy cell to 40 Hz stimulation of inhibitory fibres. *Bd*, paired-pulse depression was observed in control conditions, and LY354740 (0.5 μM) had no effect on the number of failures, uIPSC amplitudes or paired-pulse ratio. All recordings were carried out in the presence of 20 μM DNQX and 40 μM AP5 at V_h = −72 mV. Stimulation artefacts have been truncated for clarity.

Table 2. Characteristics of evoked unitary IPSCs and EPSCs

	n	Amplitude (pA)	Peak conductance (nS)	Latency (ms)	Jitter (ms)	Failure rate	Rise time (ms)	Decay τ (ms)	3rd/1st PSC	PPR	Stimulation intensity (μA)
uIPSCs	9	48.2 ± 5.84	2.40 ± 0.29	1.60 ± 0.19	0.10 ± 0.02	0.10 ± 0.04	0.61 ± 0.05	10.7 ± 0.98	0.40 ± 0.03	0.72 ± 0.02	27.7 ± 3.7
uEPSCs	8	170.2 ± 20.2	2.84 ± 0.34	1.37 ± 0.22	0.16 ± 0.01	0.37 ± 0.08	0.57 ± 0.03	4.7 ± 0.36	5.12 ± 0.49	1.44 ± 0.14	19.5 ± 4.0

Values quoted represent mean ± S.E.M. for *n* cells. Abbreviations: PPR, paired-pulse ratio; 3rd/1st PSC, ratio of amplitudes of PSC 3 to PSC 1 in a train of 40 Hz.

Time window of inhibition mediated by uIPSPs

Stimulation of mossy fibres frequently evoked action potentials superimposed on uEPSPs, especially when MCs were depolarized to between −67 mV and −62 mV (Fig. 4*Aa*, left panel), but also from the resting membrane potential (the average membrane potential in these experiments was: -70 ± 6 mV, $n = 12$). Considerable variation in action potential latency was evident, with action potentials occurring up to 80 ms after the initial stimulus. The reliability was calculated as the probability of successes, *P*(success): the number of action potentials arising from EPSPs with a latency less than 60 ms, divided by the total number of trials.

Next, uIPSPs were evoked at different time intervals from the uEPSP by minimal stimulation of inhibitory fibres in the granule cell layer. Seven cells were investigated using minimal stimulation. Since it was sometimes difficult to isolate uncontaminated uEPSCs from uIPSCs, we decided to study additional cells with a combination of minimal stimulation and dynamic clamp ($n = 5$), where uEPSP conductances were injected into the MC and paired with uIPSPs that were evoked by minimal stimulation. Since the two datasets did not give significantly different results ($P > 0.05$ for all comparisons, *t* test for independent samples and Mann–Whitney test), the data have been pooled. uIPSPs had two effects depending on their time-locking with the uEPSP. Firstly, uIPSPs were observed to exert a strong control over the reliability of EPSP–action potential coupling, significantly reducing it when the interval between uIPSP and uEPSP (Δtime) was between −10 ms and +2 ms ($P < 0.01$ or 0.001 as labelled in Fig. 4*C*, ANOVA with Bonferroni *post hoc* comparison). See Fig. 4*A* and *B* for individual cell data, and Fig. 4*C*, left graph, for pooled data. Secondly, the precision of EPSP–action potential coupling was enhanced when uIPSPs followed uEPSPs. Accordingly, this was observed by a change in the distribution of action potential latencies, although no significant differences were observed (ANOVA test, Fig. 4*A* for individual cell data, and Fig. 4*C*, middle graph, for pooled data). However, the, jitter, or standard deviation of action potential latency, was significantly depressed when uIPSPs were applied 5 ms after the uEPSP ($P < 0.05$, Kruskal–Wallis test, with Dunn's *post hoc* comparison for unequal groups, Fig. 4*C*, right graph).

Taken together, these results demonstrate that hyperpolarizing uIPSCs impose strong inhibitory control on MCs, and can depress MC reliability but enhance precision, depending on the relative timing of excitatory and inhibitory conductances.

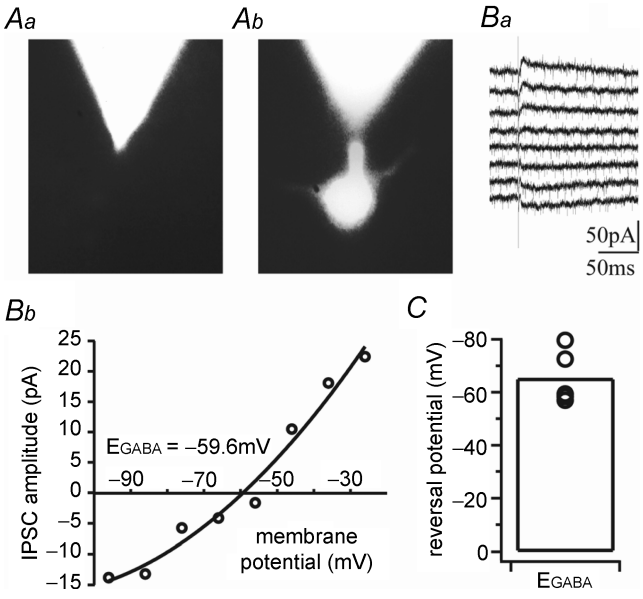

Figure 3. Reversal potential of evoked IPSCs in hilar MCs
A, epifluorescence image of the gramicidin-D perforated configuration. *Aa*, Alexa 594 is confined to the recording pipette, indicating the integrity of the perforated configuration. *Ab*, rupture of the perforated patch was confirmed by diffusion of the fluorophore into the cell body. *B*, an example of E_{GABA} measurement from the MC shown in *A*. *Ba*, traces showing IPSPs evoked at holding potentials between −100 mV and −20 mV. *Bb*, *I–V* relationship of IPSCs shown in *Ba*. The reversal potential, or E_{GABA}, was determined by fitting the data points with a second-order polynomial and interpolating to zero. In this case $E_{GABA} = -59.6$ mV. *C*, bar chart of pooled data for E_{GABA} from five cells, where each symbol refers to data from a single recorded neuron and the bar represents the arithmetic mean.

The effect of trains of uIPSPs on MC gain and offset

GABAergic interneurons have been observed to fire rhythmically in synchronization with theta frequency

oscillations, which are commonly observed in the hippocampus, including the dentate gyrus (Buzsaki, 2002). Therefore, we addressed the role that theta frequency trains of IPSPs play in modulating MC output.

Unitary IPSCs/IPSPs were evoked in a postsynaptic MC and characterized as described above (Fig. 5*A*). Then, tonic depolarizing steps of current were injected into the MC, and the mean firing frequency calculated for the duration of the pulse and plotted against the size of

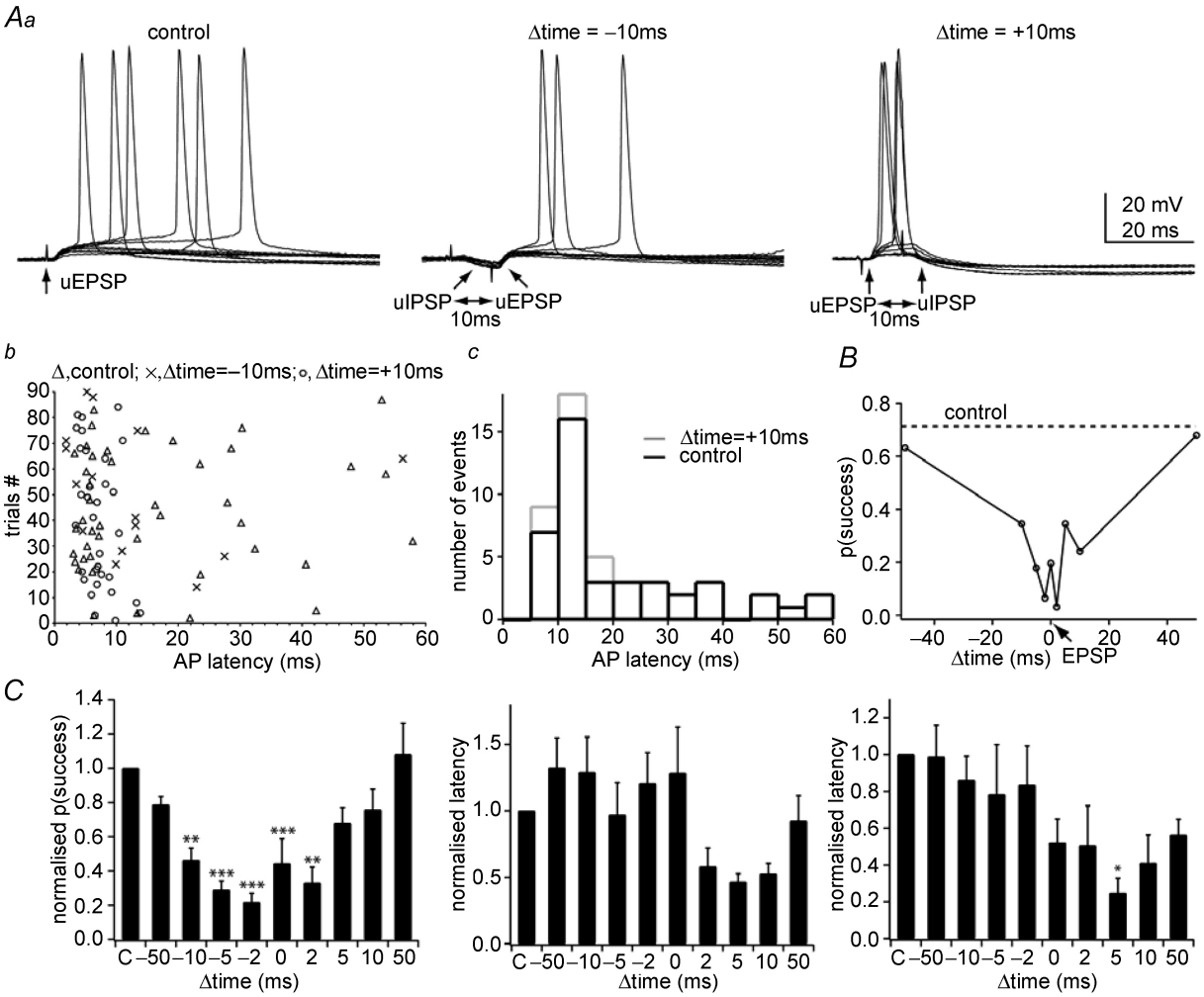

Figure 4. Time window of uIPSP-mediated inhibiton of uEPSP-action potential coupling
A, example traces of responses of a single MC to stimulation of uIPSPs and uEPSPs. Left, stimulation of mossy fibres under control conditions frequently evoked action potentials (in this cell the membrane potential was depolarized to −62 mV, *P*(success) was 0.48). Middle, pairing uEPSPs after uIPSPs with a 10 ms delay decreased the probability of EPSP–action potential coupling (*P*(success) was 0.17). Right, stimulation of uIPSPs 10 ms after uEPSPs decreased *P*(success) to 0.35, but also enhanced the precision of spike timing (latency was 17.1 ± 2.4 ms in control and 7.1 ± 0.5 ms with uIPSPs 10 ms after uEPSPs). *P*(success) values were calculated from 90 sweeps for each condition. *Ab*, rastergram of the distribution of action potential (AP) latencies in control and when a uIPSP was stimulated ±10 ms after the uEPSP in the cell shown above. *Ac*, histogram of the distribution of action potential (AP) latencies in control and when a uIPSP was stimulated 10 ms after the uEPSP in the cell shown above. Again, note that the uIPSP after uEPSP enhances spike precision. *B*, graph of *P*(success) *versus* Δtime, the delay between uEPSP and uIPSP stimulation, from another representative experiment. The uEPSP was always applied at 0 ms. Negative Δtime values denote that the uIPSP was applied before the uEPSP, conversely positive values indicate that the uIPSP was applied after the uEPSP. *C*, pooled data. Bar charts of Δtime *versus* *P*(success), latency and jitter, normalized to control values gained from files with uEPSP stimulation alone ('C' on horizontal axis). Bars represent the mean ± S.E.M. ($n = 4$–10 for each point). *, **, *** represent significance at $P < 0.05$, $P < 0.01$ and $P < 0.001$, respectively, ANOVA for Fig. 3*C* left, Kruskal–Wallis for Fig. 3*C* right. The statistical comparisons have been performed on non-normalized data.

the injected current to generate an input–output (*I–O*) curve (Fig. 5*B* and *C*). The *I–O* curve was fitted over a range of firing frequencies with equations describing a logarithmic function, as shown in Mitchell & Silver (2003) (see Methods). This enabled the determination of neuronal gain, which is represented by the slope of the *I–O* curve over the whole range of the curve fitting, and the separation of gain from the *x*-offset, or the amount of current required to bring the cell to fire. The protocol was repeated during simultaneous minimal stimulation of trains of uIPSPs at 10 Hz, and a second *I–O* curve was generated (Fig. 5*B* and *C*). We found that the train of uIPSPs increased the offset of the *I–O* relationship and surprisingly also enhanced MC gain. Furthermore, inspection of an enlargement of the voltage response under both conditions (Fig. 5*Bb*) revealed that application of 10 Hz uIPSPs increased the slope of the prepotential voltage trajectory. These effects were reversed by application of the $GABA_A$ antagonist gabazine (1.2 μM), suggesting that they were mediated by GABAergic transmission. Pooled data ($n = 7$) confirmed that 10 Hz uIPSPs increased MC gain (control: 4.89 ± 0.75 Hz pA^{-1}, 10 Hz uIPSPs: 6.29 ± 1.28 Hz pA^{-1}), offset (control: 18.46 ± 5.46 pA, 10 Hz uIPSPs: 48.09 ± 6.92 pA), maximal firing frequency (control: 10.53 ± 0.92 Hz, 10 Hz uIPSPs: 13.25 ± 1.65 Hz) and prepotential slope

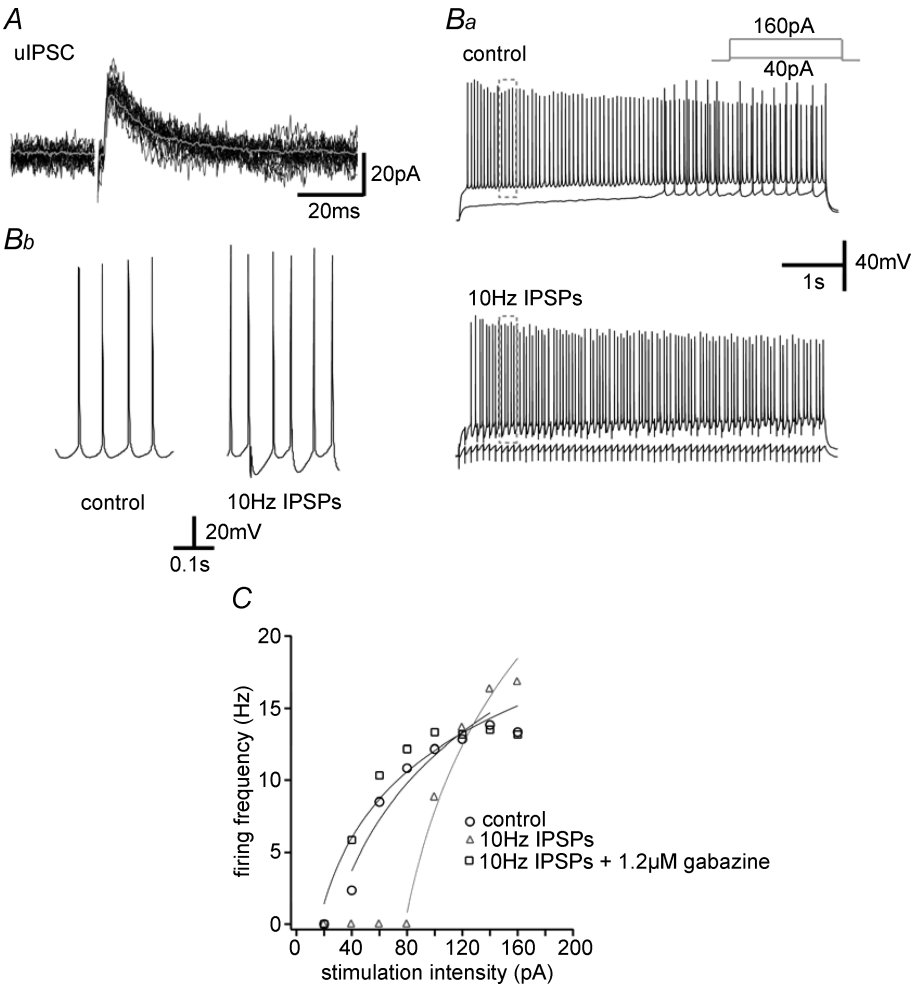

Figure 5. Effect of trains of uIPSPs on the input–output characteristics of mossy cells
A, uIPSCs were evoked by minimal stimulation in the granule cell layer (black traces, single sweeps; grey trace average). *Ba*, upper trace, response of MC to injection of tonic current steps. Lower trace, response of MC to identical current steps, but with simultaneous application of 10 Hz uIPSPs throughout current injection (6 s). Inset shows the current step protocol. *Bb*, expansion of traces displayed within grey boxes in *Ba*, to show prepotential voltage trajectory and action potential kinetics. *C*, a plot of injected current (stimulation intensity) *versus* firing frequency gives the input–output (*I–O*) relationship of the mossy cell (gain, 8.77 Hz pA^{-1}, offset, 26.30 pA). Note that application of 10 Hz uIPSPs shifts the curve to the right (increases the offset), but also increases the slope, or gain, of the *I–O* relationship (gain, 13.08 Hz pA^{-1}, offset, 78.39 pA). The effect is reversed by blocking uIPSPs with the $GABA_A$ antagonist gabazine (1.2 μM) (gain, 6.62 Hz pA^{-1}, offset, 16.16 pA).

($n = 6$, control: 76.7 ± 7.60 mV s^{-1}, 10 Hz uIPSPs: 173.3 ± 8.43 mV s^{-1}) (Fig. 6, all $P < 0.05$, Wilcoxon signed ranks test).

These results show that although uIPSPs effectively inhibit MC firing, trains of uIPSPs can also enhance the responsiveness of MCs to stimulation with tonic depolarizing current. What is the mechanism underlying this phenomenon? The observed change in prepotential voltage trajectory suggested that uIPSPs were somehow interacting with intrinsic membrane conductances, such that in the presence of uIPSPs the membrane depolarized to threshold quicker after an action potential than in the absence of uIPSPs. We first investigated the possibility that the hyperpolarization mediated by uIPSPs could activate hyperpolarization-activated cation channels (HCN) or deinactivate class 3 voltage-dependent Ca^{2+} (Ca_v3) channels, because these currents influence the rebound firing and maximal firing rate of other neuronal types (Huguenard, 1996; McCormick & Bal, 1997). Therefore, the protocol shown in Fig. 5*B* was repeated in the presence of the HCN antagonist ZD7288 (30 μM) or the Ca_v3 blocker mibefradil (1–5 μM). These antagonists, however, failed to block the uIPSP-mediated increase in MC gain. On average, the gain was 4.5 ± 1.1 Hz pA^{-1} before, and 7.3 ± 1.3 Hz pA^{-1} during, the application of uIPSPs in the presence of ZD7288 ($n = 3$), and 4.3 ± 0.3 Hz pA^{-1} before, and 7.8 ± 2.1 Hz pA^{-1} during, the application of uIPSPs in the presence of mibefradil ($n = 3$) (not shown). Next, we hypothesized that the synaptically evoked uIPSPs could interact with intrinsic Na^+ conductances.

We reasoned that the tonic depolarization by the current pulse and the sustained action potential firing during the depolarization would have caused some inactivation of the transient Na^+ current underlying the action potential (I_{Na}). The transient hyperpolarization mediated by uIPSPs would have recovered I_{Na} from an inactivating state and increased the availability of Na^+ channels for subsequent action potential generation. This mechanism has been recently shown to operate in neurons of the subthalamic nucleus (Baufreton *et al.* 2005). Consistent with this hypothesis, the action potential height, which is affected by I_{Na} inactivation (Hodgkin & Huxley, 1952) was bigger when evoked after uIPSPs than when elicited without uIPSPs for each neuron studied (Fig. 7*A*). For this analysis, we used a depolarizing current pulse of intensity that evoked more action potentials with uIPSPs than without uIPSPs (151 ± 13 pA, $n = 7$), and therefore was responsible for the uIPSP-mediated increase in the gain. On average, the action potential height evoked by the control depolarizing current pulse was 64.8 ± 2.5 mV, and by a subsequent depolarizing current pulse of the same intensity with 10 Hz uIPSPs was 68.6 ± 1.8 mV ($P < 0.05$, $n = 7$, Wilcoxon signed ranks test). Likewise, the action potential height evoked by the same depolarizing current pulses was 63.2 ± 1.5 mV when action potentials were not immediately preceded by IPSPs, and 68.6 ± 1.8 mV when immediately preceded by uIPSPs ($P < 0.05$, $n = 7$, Wilcoxon signed ranks test). Care was taken to keep the resting membrane potential stable throughout the acquisition of the data, and on average it was -81.9 ± 1.9 mV just before the control depolarizing current pulses and -82.0 ± 2.1 mV just before the depolarizing current pulses with uIPSPs ($P > 0.05$, $n = 7$, Wilcoxon signed ranks test). These results were confirmed by analysing, in the same experiments, the temporal first derivative of the membrane potential, which is a reliable estimator of I_{Na} inactivation (Hodgkin & Huxley, 1952), but unlike the action potential peak is not subject to changes in the Na^+ reversal potential. The maximal voltage of the differentiated trace (first derivative), thus the maximal slope of the action potential, was, on average, 63.9 ± 2.5 mV ms^{-1} in the control and 69.3 ± 1.8 mV ms^{-1} with 10 Hz uIPSPs (Fig. 7*B*, $P < 0.05$, $n = 7$, Wilcoxon signed ranks test). Likewise, when the action potentials were evoked by the same depolarizing current pulses, the maximal slope was 60 ± 3.6 mV ms^{-1} when IPSPs did not, and 69.3 ± 1.8 mV ms^{-1} when uIPSPs did, precede action potentials ($P < 0.05$, $n = 7$, Wilcoxon signed ranks test). This hypothesis was also tested by studying the action of TTX on the uIPSP conductance

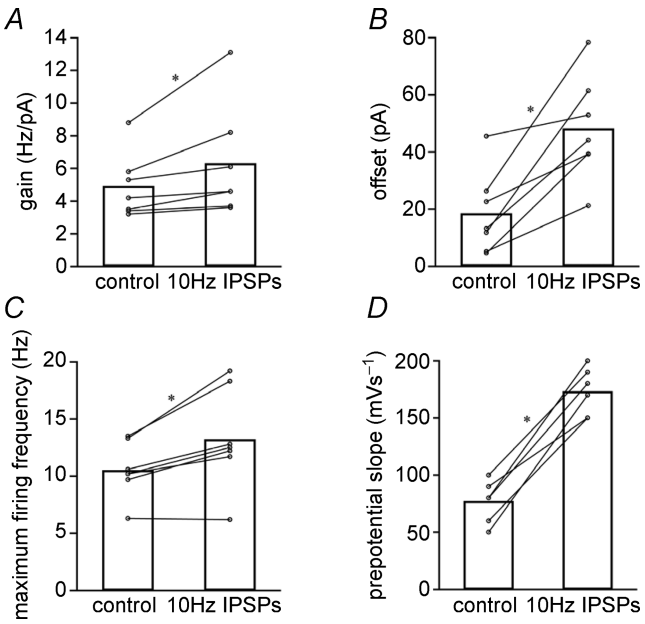

Figure 6. Pooled data illustrating the effect of trains of uIPSPs on the input–output characteristics of MCs
Charts from pooled data of gain (*A*), offset (*B*), maximum firing frequency (*C*) and prepotential slope (*D*) in control conditions and in the presence of 10 Hz IPSPs. Note that application of uIPSPs increases the gain, offset, maximum firing frequency and prepotential slope. In the graphs, each symbol refers to data from a single recorded neuron, and * represents significance ($P < 0.05$, Wilcoxon signed ranks test).

injected by dynamic clamp mode (dIPSP) into MCs that were held at subthreshold membrane potential for several seconds to increase the probability of I_{Na} inactivation (range −52 mV to −62 mV). TTX (1 μM) significantly enhanced the integral of dIPSPs (Fig. 7*C*, $P < 0.05$, $n = 5$, Wilcoxon signed ranks test), by slowing the decay without affecting the amplitude of the dIPSP. Taken together, these results suggest that uIPSPs transiently de-inactivate voltage-dependent Na^+ channels (Na_v) and enhance their open probability, leading to an increase in MC firing.

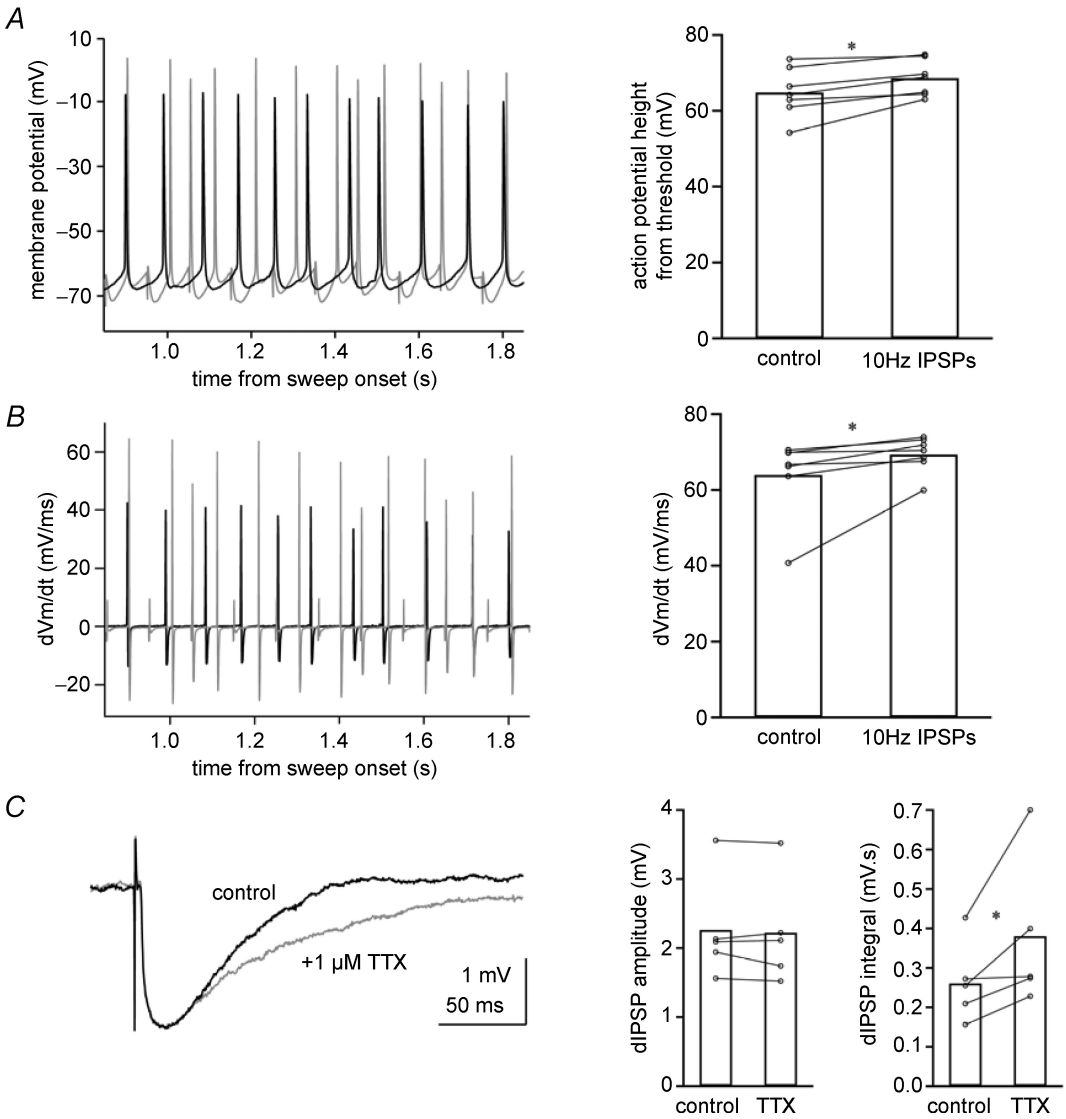

Figure 7. I_{Na} deinactivation is implicated in the increase in MC maximum firing rate induced by 10 Hz uIPSPs

A, left, action potentials in response to the injection of depolarizing current pulses (200 pA, 6 s) in control (black trace) and during 10 Hz uIPSPs (grey trace, superimposed). The height of the action potentials elicited after the uIPSPs was bigger (in this cell: 63.0 mV) than those elicited in control (54.2 mV). The resting membrane potential immediately before the depolarizing pulse was −78.6 mV in control and −78.9 mV with 10 Hz IPSPs. In the *x* axis, seconds (s) refer to the time after the onset of the sweeps (the onset of the depolarizing current pulse was 45 ms after the onset of the sweeps). Right graph, pooled data, each symbol refers to data from a single recorded neuron, * represents significance ($P < 0.05$, $n = 7$, Wilcoxon signed ranks test). *B*, first derivative *versus* time of the traces shown in *A*. In this example, the maximal height of the differentiated action potential was 40.7 mV ms^{-1} in the control (black trace) and 59.9 mV ms^{-1} with 10 Hz uIPSPs (grey trace). Right graph, pooled data, each symbol refers to data from each recorded neuron, * represents significance ($P < 0.05$, $n = 7$, Wilcoxon signed ranks test). *C*, left, dIPSPs before or during bath application of TTX. Right, pooled data of the amplitude and integral of dIPSPs before or during bath application of TTX, each symbol refers to data from a single recorded neuron, * represents significance ($P < 0.05$, $n = 5$, Wilcoxon signed ranks test).

Functional consequences

The results shown indicate that uIPSPs not only depressed MC excitability, but also enhanced the gain and the maximum firing rate of action potentials during tonic MC depolarization. Under which conditions may these effects occur? Cholinergic septohippocampal fibres heavily innervate hilar MCs (Deller *et al.* 1999) and the muscarinic agonist pilocarpine directly depolarizes hilar GABAergic interneurons and MCs in hippocampal slice cultures (Thomas *et al.* 2005). Therefore, we hypothesized that pilocarpine could enhance the synaptic inhibition impinging on MCs, by directly depolarizing hilar interneurons, and this could enhance Na^+ channel recovery from inactivation, and thus increase the firing of the depolarized MCs. In order to test this hypothesis, first, we tested whether the application of pilocarpine (0.5 mM, 10 min) directly activated hilar interneurons in acute slices. Pilocarpine depolarized and induced action potentials in all seven hilar non-fast-spiking interneurons and in three out of five hilar fast-spiking interneurons tested (Fig. 8*A* and *B*). All interneurons were silent before the

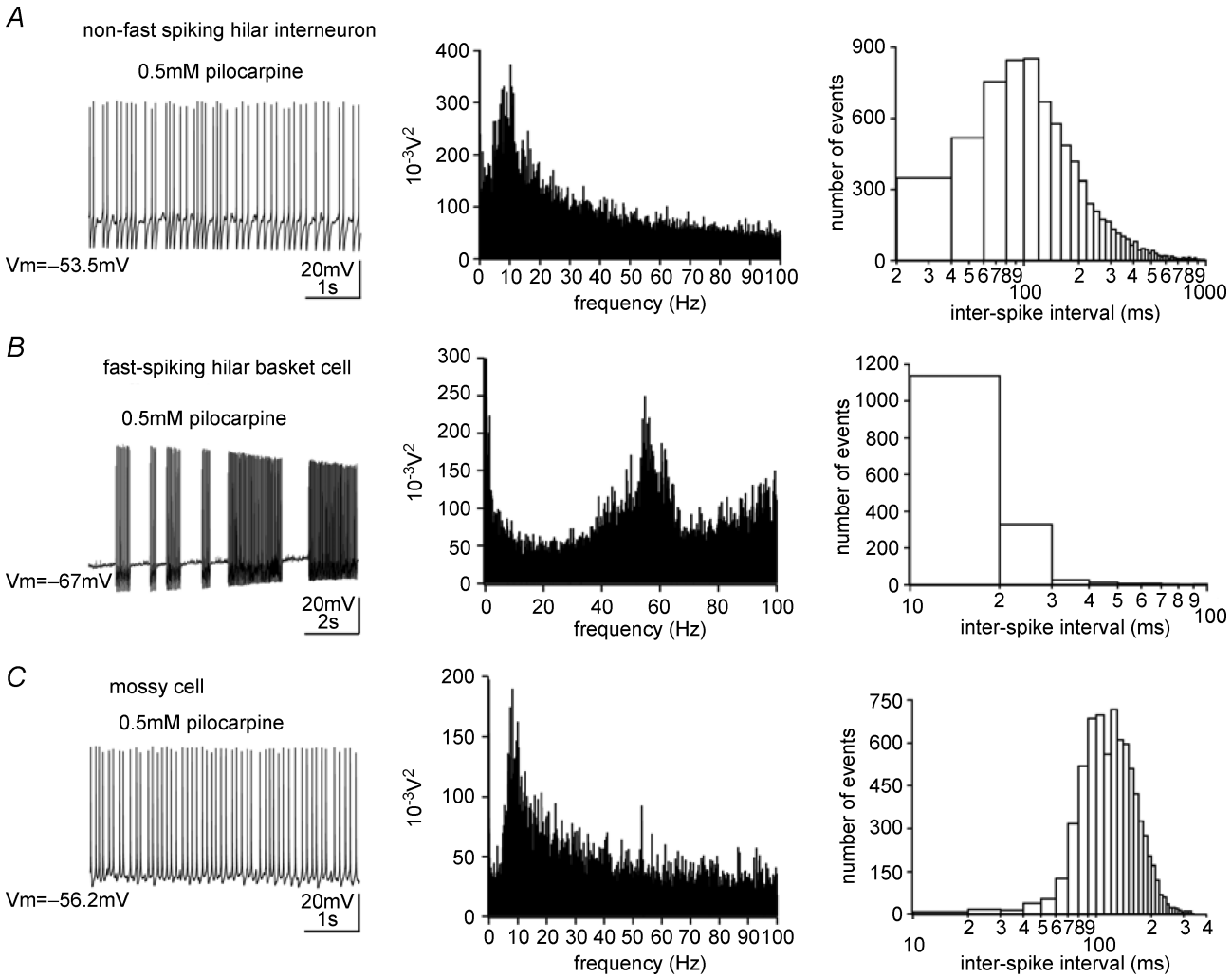

Figure 8. Pilocarpine induces firing in hilar interneurons and in MCs
A, pilocarpine (0.5 mM) directly depolarized and evoked action potentials in a non-fast-spiking hilar interneuron (left). The power of activity of the cell shown peaked at around 10 Hz (middle), and the log-binning plot (bin = 20 ms) of the interspike intervals for the pooled data peaked at around 100 ms ($n = 7$, right). *B*, pilocarpine (0.5 mM) directly depolarized and evoked action potentials in a hilar fast-spiking neuron (left). The action potentials occurred in bursts and in tonic mode at several different frequencies, as shown by the plot of the power spectral analysis of the firing of the cell shown (middle) and by the log-binning plot (bin = 10 ms) of the interspike intervals (pooled data, $n = 3$, right). *C*, pilocarpine (0.5 mM) depolarized and elicited action potentials in MCs, applied in the presence of DNQX (20 μM) and AP5 (40 μM). The power of activity of the cell shown peaked at around 10 Hz (middle), and the log-binning plot (bin = 10 ms) of the interspike intervals peaked at around 100 ms (pooled data, $n = 7$, right). V_m next to the traces indicates the resting membrane potential.

application of the drug. Analysis of the action potential interevent interval revealed that action potentials were evoked in tonic mode with a main frequency of 10 Hz in the regular spiking interneurons and in burst and in tonic mode with frequencies >10 Hz in the fast-spiking interneurons (Fig. 8*A* and *B*). Next, pilocarpine (0.5 mM) was applied to MCs, in the presence of the ionotropic glutamate receptor antagonists DNQX (20 μM) and AP5 (40 μM) to isolate the contribution of the GABAergic inputs. Pilocarpine induced a clear-cut occurrence of IPSPs (Figs 8*C*, 9*Ac* and 9*Ae*), consistent with its excitation of hilar interneurons and their innervation of MCs.

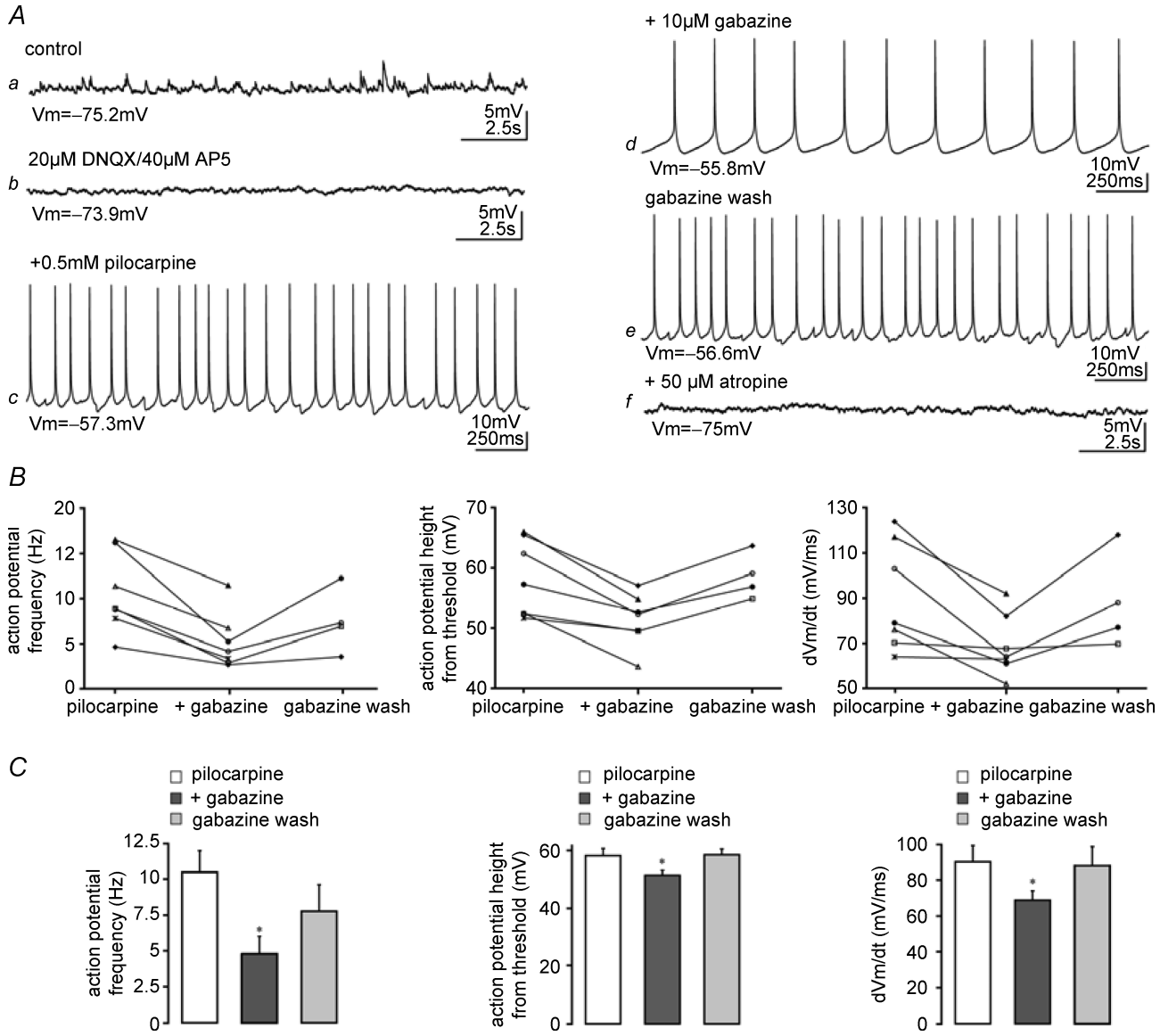

Figure 9. IPSPs contribute to the increase of MC firing induced by the cholinergic agonist pilocarpine
A, pilocarpine depolarized and elicited action potentials in MCs. The traces are continuous current clamp recordings in a MC in control (*a*), during application of 20 μM DNQX/40 μM AP5 (*b*), pilocarpine (0.5 mM, 2 min, trace *c*), gabazine (10 μM, 2 min, trace *d*), washout of gabazine (trace *e*), and atropine (50 μM, trace *f*). The membrane potential (V_m) for each condition is indicated next to each trace. Note that several IPSPs were present during pilocarpine application often immediately preceding action potentials (traces *c* and *e*). In the presence of pilocarpine, application of gabazine reduced the frequency and the peak amplitude of action potentials. The effect of gabazine was reversed upon washout of the drug, and atropine blocked the action of pilocarpine. *B* and *C*, plots of action potential mean frequency (left), height (middle) and maximal slope (right) in pilocarpine ($n = 7$), pilocarpine and gabazine ($n = 7$) and after washout of gabazine ($n = 4$), for each neuron tested (*B*) and pooled data (*C*), showing mean ± S.E.M. values. Each symbol refers to data from each recorded neuron and * represents significance *versus* control ($n = 7$, $P < 0.05$, Wilcoxon signed ranks test).

Pilocarpine also depolarized MCs and induced sustained action potentials at a main frequency of 10Hz (Figs 8*C*, 9*Ac*, 9*B* and 9*C*). Interestingly, IPSPs often preceded these action potentials, leading the membrane to active firing (Figs 8*C*, 9*Ac* and 9*Ae*). Under these conditions, applications of the $GABA_A$ antagonist gabazine (10 μM) blocked the IPSPs without significantly changing the tonic depolarization induced by pilocarpine. Interestingly, the frequency of action potentials observed in the presence of gabazine and pilocarpine was less then that previously detected with pilocarpine alone (Fig. 9*Ad*). Furthermore, the action potential height was less in the presence of gabazine and pilocarpine than with pilocarpine alone (Fig. 9*Ad*). Washout of gabazine reversed its effects (Fig. 9*Ae*), and addition of atropine (50 μM) abolished all the effects elicited by pilocarpine (Fig. 9*Af*). These observations were confirmed in six other recordings, and pooled data for the action of pilocarpine without and with gabazine on action potential frequency and height are summarized in Fig. 9*B* and *C* ($P < 0.05$ for all comparisons, Wilkoxon signed ranks test, $n = 7$). Moreover, an analysis of the temporal first derivative of the membrane potential revealed that the maximal slope of the action potentials induced by pilocarpine was also significantly decreased by gabazine (Fig. 9*B* and *C*, $P < 0.05$, Wilkoxon signed ranks test, $n = 7$). In these experiments, the resting membrane potential was -75 ± 0.6 mV in the control ($n = 7$), -73.6 ± 1 mV in DNQX/AP5 ($n = 7$), -53 ± 1.2 mV with DNQX/AP5 and pilocarpine ($n = 7$), -51.5 ± 1.5 mV in DNQX/AP5, pilocarpine and gabazine ($n = 7$), and -71.4 ± 0.8 mV with DNQX/AP5, pilocarpine, gabazine and atropine. The mean values of the resting membrane potential in pilocarpine and DNQX/AP5 or gabazine, pilocarpine and DNQX/AP5 were significantly different compared to the control value ($P < 0.05$ for both, Kruskal–Wallis test) but not from each other ($P > 0.05$, Kruskal–Wallis test). Thus, the prolonged activation of cholinergic inputs to the dentate gyrus could contribute to the uIPSC-mediated increase in MC gain.

Discussion

This work describes novel mechanisms underlying the GABAergic control of neuronal integration by recording from hippocampal hilar MCs as a model system. We show that uIPSCs are capable of silencing the mossy fibre–MC synapse over a considerable time window. Surprisingly, stimulation of uIPSPs can also tune into the resonance frequency of MCs and enhance MC gain. We propose that this phenomenon is due to the IPSP-mediated transient hyperpolarization that enhances Na^+ channel recovery from inactivation and increases the maximal firing frequency over a range of depolarizing tonic current steps. Thus, GABAergic conductances do not solely have an inhibitory function, but can also enhance the responsiveness of MCs to a given excitatory input.

The unitary nature of synaptic events evoked by minimal stimulation

Minimal stimulation was employed in this study to investigate unitary synaptic transmission, because in preliminary experiments no synaptically coupled pairs were observed (authors' unpublished observations). The plot of amplitude *versus* stimulation intensity for all uEPSCs included in this study showed a sharp increase to a plateau mean amplitude value. Moreover, all uEPSCs displayed fast rise time kinetics and were readily depressed by the application of the group II mGluR agonist LY354740, lending further credence to their origin from a single presynaptic mossy fibre. The uEPSCs we observed had larger amplitudes than those described in CA3 pyramids and MCs, by Jonas *et al.* (1993) and Lysetskiy *et al.* (2005), respectively. This could be due to the higher Ca^{2+}/Mg^{2+} ratio in our ACSF and larger input resistance of MCs as compared to CA3 pyramids. Previously, paired recordings with sharp microelectrodes have revealed that the synapse is characterized by large-amplitude responses that can sometimes bring MCs to fire (Scharfman *et al.* 1990). More recently, we have described uEPSCs between granule cells and MCs in organotypic slice cultures obtained with double-patch recordings, and the amplitudes measured under these conditions (173.9 ± 83.0 pA in slice cultures, Thomas *et al.* 2005) were almost identical to uEPSCs evoked by minimal stimulation in the present study (170.2 ± 20.2 pA in acute slices). Moreover, uEPSCs in MCs displayed short-term facilitation, in agreement with recently published data showing facilitation of mossy fibre-mediated uEPSCs onto MCs (Lysetskiy *et al.* 2005). Anatomical studies have shown that mossy fibres terminate on the complex spines of MC proximal dendrites (Claiborne *et al.* 1986; Acsády *et al.* 1998), a site where space-clamp problems should be small.

Minimal stimulation of fibres in the granule cell layer evoked all-or-none IPSCs in MCs at low stimulation intensities. All IPSCs investigated conformed to the criteria outlined above for identification of single fibre stimulation, and also displayed fast rise time kinetics. Furthermore the standard deviation of amplitudes for each cell was very small (<15 pA). The identity of the inhibitory synaptic inputs under investigation is not known. However, anatomical studies suggest that, in addition to inputs from axo-axonic cells (Halasy & Somogyi, 1993), MCs receive perisomatic synapses from both regular-spiking cholecystokinin-positive and fast-spiking parvalbumin-positive basket cells (Acsády *et al.* 2000). Together with the fast kinetics of the IPSPs that

we recorded and their effective inhibition and shunting of EPSPs, it seems likely that the uIPSCs that we record are generated at proximal locations to the soma. Moreover, the membrane domain innervated by the axo-axonic neuron is surrounded by Na^+ channels at high density and is nearby the suggested site of the action potential initiation (Colbert & Johnston, 1996). Such an arrangement therefore should also favour the tight interaction between uIPSPs and I_{Na} that we have detected in MCs. Interestingly, such an interaction, where IPSPs mediate de-inactivation of I_{Na} channels has been postulated to lead to the sublinear summation of IPSP kinetics at cortical axo-axonic neuron to layer 4 pyramidal cell synapses (Tamas & Szabadics, 2004). Furthermore, non-fast-spiking hilar interneurons fired action potentials at similar frequencies to MCs after pilocarpine application, and this is consistent with the presence of axon collaterals in the hilus from several hilar interneurons that could entrain MCs (Han *et al.* 1993; Lubke *et al.* 1998).

Single IPSPs effectively control EPSP–action potential coupling in MCs

Our data shows that uIPSPs can reduce the efficacy and enhance the precision of EPSP–action potential coupling over a range of several milliseconds, in agreement with previous studies in other cell types (Cobb *et al.* 1995; Kim *et al.* 1995; Bevan *et al.* 2002; Carter & Regehr, 2002; Williams & Stuart, 2003; Person & Perkel, 2005).

Furthermore, we show that the reversal potential for $GABA_A$-mediated currents in MCs, or E_{GABA} (−65.3 mV), lies between the resting membrane potential (−75.3 mV) and the action potential threshold (−56.5 mV). Thus, at rest, IPSPs generated close to the soma are likely to modulate MC activity through shunting inhibition or subthreshold depolarization. Previously, E_{GABA} has been measured to be more positive than the resting membrane potential in other neuronal types (Liu *et al.* 1998; Martina *et al.* 2001; Chavas & Marty, 2003; Gulledge & Stuart, 2003; Vida *et al.* 2006). The intracellular chloride concentration, and thus reversal potential of E_{GABA}, is dependent on the expression and activity of transporters such as the KCl cotransporter KCC2 and the $Na^+/K^+/Cl^-$ cotransporter NKCC1 (Ben-Ari, 2002). Therefore, the observed depolarized E_{GABA} could be explained by the absence of Cl^- transporters or their downregulation. Furthermore, $GABA_A$ channels are also permeable to bicarbonate ions (Kaila, 1994), which can also contribute to depolarizing $GABA_A$-mediated currents (Kaila *et al.* 1993).

Using the Nernst equation, and assuming a permeability ratio for bicarbonate to chloride ions of 0.2, E_{GABA} in our whole-cell recordings was −90.1 mV. Thus, in all our whole-cell recordings, GABAergic currents were hyperpolarizing. We observed that hyperpolarizing uIPSPs modulated EPSP–action potential coupling. Under which physiological conditions will IPSPs be hyperpolarizing when the intracellular chloride concentration is unperturbed? MCs exhibit resting membrane potential oscillations that are phase-locked to the extracellularly recorded hippocampal theta frequency oscillations *in vivo* (Soltesz *et al.* 1993). In the so-called up-state, the membrane potential could become sufficiently depolarized to render IPSPs hyperpolarizing.

Moreover, our results suggest that the relative timing of the IPSP is also important in modulating EPSP–action potential coupling. Our data are consistent with the data of Pouille & Scanziani (2001), who showed that IPSPs that arise in a feed-forward manner can enhance the precision of spike timing in CA1 pyramidal cells. However, little evidence has been observed for synaptic feed-forward inhibition on MCs, even after perforant path stimulation, in the acute slice preparation (Scharfman & Schwartzkroin, 1988; Scharfman, 1992; Buckmaster *et al.* 1993). Synaptic inhibition of MCs, however, becomes more apparent *in vivo* (Soltesz *et al.* 1993), where feed-forward inhibition was evident after stimulation of the entorhinal cortex.

MCs are believed to be a highly vulnerable population of neurons, and it has been proposed that this is in part due to the relatively small inhibitory drive that they appear to receive in comparison with the large excitatory drive from mossy fibre and CA3 inputs (Scharfman, 1994; Buckmaster & Schwartzkroin, 1994; Ratzliff *et al.* 2002). The data provided here show that MCs receive substantial GABAergic inputs, which can control the cell firing over a time window of several milliseconds and can depolarize the cell at resting membrane potential.

Trains of uIPSPs can enhance MC gain

We also show that phasic synaptic inhibition, mediated by uIPSPs, increased MC offset, such that a larger tonic excitation was required to bring the cell to fire. Unexpectedly, however, synaptic inhibition also increased the gain, and therefore sensitivity, and maximal firing rate of MCs in response to tonic excitatory current injection. This result suggests that, over the range of 'output' firing frequencies studied in our experiments and under certain conditions, inhibition can enable MCs to respond to a given input with an increased output.

In a MC with unperturbed intracellular chloride concentration, one would expect that when small depolarizing current injections are applied to the MC soma, IPSPs would be purely shunting due to the relatively depolarized E_{GABA}. However, our results are consistent with IPSP modulation of Na_v conductances only after application of a weak depolarizing stimulus. Given the relatively high input resistance of MCs,

only about 60 pA is required to bring the membrane potential more depolarized than E_{GABA}, so after the 60 pA current injection, GABAergic currents will be solely hyperpolarizing. Thus, even with physiological intracellular chloride concentrations, maximal firing rate, action potential height and the maximal slope of the differentiated trace could still increase during the application of 10 Hz hyperpolarizing IPSPs.

In our whole-cell experiments, the height and the maximal slope of the action potentials immediately after IPSPs were significantly higher than that evoked at the same membrane potential without IPSPs, suggesting that Na_v channels underlie this phenomenon. The speed of recovery from inactivation of Na_v channels is exponentially dependent on the hyperpolarization of the membrane after depolarization (Ketelaars *et al.* 2001). Our data shows that uIPSPs provide an enhanced hyperpolarization immediately before action potentials, thus de-inactivating a greater proportion of subthreshold Na_v channels, allowing more rapid depolarization of the membrane to threshold, and consequently inducing rebound action potentials with a shorter inter-action potential interval. This interpretation is in agreement with our finding that the slope of the prepotential was enhanced in the presence of inhibition and with the slower decay and larger integral of dIPSPs in the presence of TTX as opposed to controls. A recent study has observed a similar phenomenon in subthalamic nucleus neurons, whereby IPSPs enhanced postsynaptic Na_v channel availability, actively truncating synthetic IPSPs and dramatically improving EPSP–action potential coupling (Baufreton *et al.* 2005). Resurgent Na^+ channels have also been observed to contribute to the fast-spiking phenotype of cerebellar Purkinje neurons (Raman & Bean, 1997) and subthalamic neurons (Do & Bean, 2003), and in principle the opening probability of these channels could have been increased by uIPSPs, generating a more rapid depolarization of the membrane to threshold (Raman & Bean, 1997). However, it is not known whether resurgent Na^+ channels are present in MCs, and we have not investigated whether this conductance also contributed to the uIPSP-mediated effect. It is unlikely that uIPSPs interacted with a persistent Na^+ current (I_{NaP}), because this current was largely absent in our non-bursting MCs, in agreement with a previous report in mice MCs (Jinno *et al.* 2003). As shown in layer V pyramidal neurons, I_{NaP} prolongs IPSPs (Stuart, 1999), and therefore the interaction of these channels with uIPSPs would decrease the firing rate and not increase it, as we have observed. Recent data also showed that I_{NaP} reduces the gain and decreases the spike time precision of CA1 pyramidal neurons (Vervaeke *et al.* 2006), thus both effects are just the opposite of those we report here in MCs. Furthermore, our results do not support an interaction between IPSPs and HCN or Ca_v3 channels, which have been shown to modulate the rebound firing and maximal firing rate of other neuronal types (Huguenard, 1996; McCormick & Bal, 1997), since specific antagonists for these channels did not affect the uIPSP-induced increase in MC gain.

Previous studies of *I–O* relationships in various neuronal types have shown that inhibition always shifts the offset such that a greater excitatory input is required for the cell to generate any output. However, inhibition has been previously described to either have no effect on, or depress the gain of *I–O* relationships (Granit *et al.* 1966; Berman *et al.* 1992; Brickley *et al.* 1996; Mitchell & Silver, 2003; Morita *et al.* 2005). In contrast, we observed that inhibitory synaptic inputs can actually enhance the gain and sensitivity of neurons, and perhaps this could be due to a differential modulation of membrane conductances when hyperpolarizing IPSPs are applied, as in our study, and shunting IPSPs or IPSPs with a depolarized E_{GABA}, as previously reported (Mitchell & Silver, 2003; Morita *et al.* 2005). Our experimental data show that a continuous firing, for example within the theta frequency range, of dentate interneurons could enhance MC excitability, such that they translate granule cell inputs into a greater output.

In the anaesthetized rat *in vivo*, MCs exhibit resting membrane potential oscillations that are phase-locked to the extracellularly recorded hippocampal theta frequency oscillations, and rhythmic $GABA_A$ receptor-mediated events contribute to the genesis of this intracellular rhythm (Soltesz *et al.* 1993). Although the firing patterns of MCs in non-anaesthetized rats are not known, bistability of the membrane potential is likely to occur, and under these conditions inhibitory inputs may not only increase the offset but also enhance the gain of MCs, as we have described here *in vitro*. However, while we focus on the theta frequency IPSP modulation of MC gain in response to tonic depolarizing steps, the modulation of MC gain mediated by phasic EPSPs and IPSPs of different or varying frequencies is beyond the scope of the present study.

The increase in the gain and maximal firing rate is also likely to be relevant for MCs under pathological conditions. Here, we show that pilocarpine application induced a tonic depolarization and firing at a main frequency of 10 Hz in MCs and hilar non-fast-spiking interneurons, but elicited higher-frequency firing in three out of five fast-spiking hilar interneurons. Thus pilocarpine mimicked the tonic depolarizing current steps and IPSPs applied at 10Hz in the *I–O* experiments, and consequently enhanced MC output. This is consistent with the direct pilocarpine-mediated depolarization of MCs that we have previously reported in the presence of TTX (Thomas *et al.* 2005). We believe that this direct depolarization via MC intrinsic membrane conductances is a major factor in the pilocarpine-induced excitation of MCs. However, the uIPSP-induced increase in MC gain

and de-inactivation of Na_v channels are also likely to contribute to the excitatory action of pilocarpine, since pilocarpine largely increased the occurrence of IPSPs, and addition of gabazine reduced the frequency, the amplitude and the maximal slope of the action potentials induced by pilocarpine. These effects must be independent of glutamatergic transmission, since they were observed in the presence of DNQX and AP5. This interpretation is consistent with our finding that pilocarpine depolarized MCs to values more positive than E_{GABA}, indicating that the drug-evoked IPSPs would be hyperpolarizing also when intracellular Cl^- is unperturbed. In addition, other 'excitatory' GABAergic mechanisms may also contribute to the decrease of excitability after blocking $GABA_A$ receptors. For example, an excitatory action of axo-axonic cells has been recently shown, and it has been suggested that activation of this interneuron would lead to synchronous recruitment of network activity (Szabadics *et al.* 2006). As discussed above, this class of interneuron may well be involved in the effects we observed, due to their anatomical and functional specificities. Furthermore, $GABA_A$ receptors are expressed at mossy fibres and modulate the release of glutamate (Ruiz *et al.* 2003). This mechanism is likely to contribute to the changes of excitability induced by alteration of $GABA_A$ receptor function in the absence of excitatory amino acid antagonists.

Overall, our data are in support of 'the irritable MC' hypothesis proposed by Soltesz and colleagues (Santhakumar *et al.* 2000; Ratzliff *et al.* 2002; Ratzliff *et al.* 2004), postulating an active role of MCs in promoting excitation under hyperexcitable conditions. Cholinergic septohippocampal fibres heavily innervate hilar MCs (Deller *et al.* 1999) and therefore modulate their activity. The highly divergent MC output would then allow for a widespread distribution of rhythmic MC activity through large sectors of the dentate gyrus.

References

Acsády L, Kamondi A, Sik A, Freund T & Buzsaki G (1998). GABAergic cells are the major postsynaptic targets of mossy fibers in the rat hippocampus. *J Neurosci* **18**, 3386–3403.

Acsády L, Katona I, Martinez-Guijarro FJ, Buzsaki G & Freund TF (2000). Unusual target selectivity of perisomatic inhibitory cells in the hilar region of the rat hippocampus. *J Neurosci* **20**, 6907–6919.

Amaral DG (1978). A Golgi study of cell types in the hilar region of the hippocampus in the rat. *J Comp Neurol* **182**, 851–914.

Bacci A & Huguenard JR (2006). Enhancement of spike-timing precision by autaptic transmission in neocortical inhibitory interneurons. *Neuron* **49**, 119–130.

Bartos M, Vida I, Frotscher M, Geiger JR & Jonas P (2001). Rapid signaling at inhibitory synapses in a dentate gyrus interneuron network. *J Neurosci* **21**, 2687–2698.

Baufreton J, Atherton JF, Surmeier DJ & Bevan MD (2005). Enhancement of excitatory synaptic integration by GABAergic inhibition in the subthalamic nucleus. *J Neurosci* **25**, 8505–8517.

Ben-Ari Y (2002). Excitatory actions of gaba during development: the nature of the nurture. *Nat Rev Neurosci* **3**, 728–739.

Berman NJ, Douglas RJ & Martin KA (1992). GABA-mediated inhibition in the neural networks of visual cortex. *Prog Brain Res* **90**, 443–476.

Bevan MD, Magill PJ, Hallworth NE, Bolam JP & Wilson CJ (2002). Regulation of the timing and pattern of action potential generation in rat subthalamic neurons in vitro by GABA-A IPSPs. *J Neurophysiol* **87**, 1348–1362.

Brickley SG, Cull-Candy SG & Farrant M (1996). Development of a tonic form of synaptic inhibition in rat cerebellar granule cells resulting from persistent activation of $GABA_A$ receptors. *J Physiol* **497**, 753–759.

Buckmaster PS & Schwartzkroin PA (1994). Hippocampal mossy cell function: a speculative view. *Hippocampus* **4**, 393–402.

Buckmaster PS, Strowbridge BW & Schwartzkroin PA (1993). A comparison of rat hippocampal mossy cells and CA3c pyramidal cells. *J Neurophysiol* **70**, 1281–1299.

Buzsaki G (2002). Theta oscillations in the hippocampus. *Neuron* **33**, 325–340.

Carter AG & Regehr WG (2002). Quantal events shape cerebellar interneuron firing. *Nat Neurosci* **5**, 1309–1318.

Chavas J & Marty A (2003). Coexistence of excitatory and inhibitory GABA synapses in the cerebellar interneuron network. *J Neurosci* **23**, 2019–2031.

Claiborne BJ, Amaral DG & Cowan WM (1986). A light and electron microscopic analysis of the mossy fibers of the rat dentate gyrus. *J Comp Neurol* **246**, 435–458.

Cobb SR, Buhl EH, Halasy K, Paulsen O & Somogyi P (1995). Synchronization of neuronal activity in hippocampus by individual GABAergic interneurons. *Nature* **378**, 75–78.

Colbert CM & Johnston D (1996). Axonal action-potential initiation and Na+ channel densities in the soma and axon initial segment of subicular pyramidal neurons. *J Neurosci* **16**, 6676–6686.

Coombs JS, Eccles JC & Fatt P (1955). The inhibitory suppression of reflex discharges from motoneurones. *J Physiol* **130**, 396–413.

Deller T, Katona I, Cozzari C, Frotscher M & Freund TF (1999). Cholinergic innervation of mossy cells in the rat fascia dentata. *Hippocampus* **9**, 314–320.

Do MT & Bean BP (2003). Subthreshold sodium currents and pacemaking of subthalamic neurons: modulation by slow inactivation. *Neuron* **39**, 109–120.

Frazier CJ, Strowbridge BW & Papke RL (2003). Nicotinic receptors on local circuit neurons in dentate gyrus: a potential role in regulation of granule cell excitability. *J Neurophysiol* **89**, 3018–3028.

Fricker D & Miles R (2000). EPSP amplification and the precision of spike timing in hippocampal neurons. *Neuron* **28**, 559–569.

Frotscher M, Seress L, Schwerdtfeger WK & Buhl E (1991). The mossy cells of the fascia dentata: a comparative study of their fine structure and synaptic connections in rodents and primates. *J Comp Neurol* **312**, 145–163.

Granit R, Kernell D & Lamarre Y (1966). Algebraical summation in synaptic activation of motoneurones firing within the 'primary range' to injected currents. *J Physiol* **187**, 379–399.

Gulledge AT & Stuart GJ (2003). Excitatory actions of GABA in the cortex. *Neuron* **37**, 299–309.

Halasy K & Somogyi P (1993). Subdivisions in the multiple GABAergic innervation of granule cells in the dentate gyrus of the rat hippocampus. *Eur J Neurosci* **5**, 411–429.

Han ZS, Buhl EH, Lorinczi Z & Somogyi P (1993). A high degree of spatial selectivity in the axonal and dendritic domains of physiologically identified local-circuit neurons in the dentate gyrus of the rat hippocampus. *Eur J Neurosci* **5**, 395–410.

Hodgkin AL & Huxley AF (1952). A quantitative description of membrane current and its application to conduction and excitation in nerve. *J Physiol* **117**, 500–544.

Holt GR & Koch C (1997). Shunting inhibition does not have a divisive effect on firing rates. *Neural Computat* **9**, 1001–1013.

Huguenard JR (1996). Low-threshold calcium currents in central nervous system neurons. *Annu Rev Physiol* **58**, 329–348.

Hunter JD, Milton JG, Thomas PJ & Cowan JD (1998). Resonance effect for neural spike time reliability. *J Neurophysiol* **80**, 1427–1438.

Jinno S, Ishizuka S & Kosaka T (2003). Ionic currents underlying rhythmic bursting of ventral mossy cells in the developing mouse dentate gyrus. *Eur J Neurosci* **17**, 1338–1354.

Jonas P, Major G & Sakmann B (1993). Quantal components of unitary EPSCs at the mossy fibre synapse on CA3 pyramidal cells of rat hippocampus. *J Physiol* **472**, 615–663.

Kaila K (1994). Ionic basis of $GABA_A$ receptor channel function in the nervous system. *Prog Neurobiol* **42**, 489–537.

Kaila K, Voipio J, Paalasmaa P, Pasternack M & Deisz RA (1993). The role of bicarbonate in $GABA_A$ receptor-mediated IPSPs of rat neocortical neurones. *J Physiol* **464**, 273–289.

Kamiya H, Shinozaki H & Yamamoto C (1996). Activation of metabotropic glutamate receptor type 2/3 suppresses transmission at rat hippocampal mossy fibre synapses. *J Physiol* **493**, 447–455.

Ketelaars SO, Gorter JA, van Vliet EA, Lopes da Silva FH & Wadman WJ (2001). Sodium currents in isolated rat CA1 pyramidal and dentate granule neurones in the post-status epilepticus model of epilepsy. *Neuroscience* **105**, 109–120.

Kim HG, Beierlein M & Connors BW (1995). Inhibitory control of excitable dendrites in neocortex. *J Neurophysiol* **74**, 1810–1814.

Lisman JE (1999). Relating hippocampal circuitry to function: recall of memory sequences by reciprocal dentate–CA3 interactions. *Neuron* **22**, 233–242.

Liu YBYeG-L, Liu X-S, Pasternak JF & Trommer BL (1998). $GABA_A$ currents in immature dentate gyrus granule cells. *J Neurophysiol* **80**, 2255–2267.

Lubke J, Frotscher M & Spruston N (1998). Specialized electrophysiological properties of anatomically identified neurons in the hilar region of the rat fascia dentata. *J Neurophysiol* **79**, 1518–1534.

Lysetskiy M, Földy C & Soltesz I (2005). Long- and short-term plasticity at mossy fiber synapses on mossy cells in the rat dentate gyrus. *Hippocampus* **15**, 691–696.

Lytton WW & Sejnowski TJ (1991). Simulations of cortical pyramidal neurons synchronized by inhibitory interneurons. *J Neurophysiol* **66**, 1059–1079.

Martina M, Royer S & Pare D (2001). Cell-type-specific GABA responses and chloride homeostasis in the cortex and amygdala. *J Neurophysiol* **86**, 2887–2895.

Marty A & Llano I (2005). Excitatory effects of GABA in established brain networks. *Trends Neurosci* **28**, 284–289.

McCormick DA & Bal T (1997). Sleep and arousal: thalamocortical mechanisms. *Annu Rev Neurosci* **20**, 185–215.

Mitchell SJ & Silver RA (2003). Shunting inhibition modulates neuronal gain during synaptic excitation. *Neuron* **38**, 433–445.

Morita K, Tsumoto K & Aihara K (2005). Possible effects of depolarising $GABA_A$ conductance on the neuronal input–output relationship: a modelling study. *J Neurophysiol* **93**, 3504–3523.

Person AL & Perkel DJ (2005). Unitary IPSPs drive precise thalamic spiking in a circuit required for learning. *Neuron* **46**, 129–140.

Pouille F & Scanziani M (2001). Enforcement of temporal fidelity in pyramidal cells by somatic feed-forward inhibition. *Science* **293**, 1159–1163.

Pouille F & Scanziani M (2004). Routing of spike series by dynamic circuits in the hippocampus. *Nature* **429**, 717–723.

Raman IM & Bean BP (1997). Resurgent sodium current and action potential formation in dissociated cerebellar Purkinje neurons. *J Neurosci* **17**, 4517–4526.

Ratzliff AH, Howard AL, Santhakumar V, Osapay I & Soltesz I (2004). Rapid deletion of mossy cells does not result in a hyperexcitable dentate gyrus: implications for epileptogenesis. *J Neurosci* **24**, 2259–2269.

Ratzliff AH, Santhakumar V, Howard A & Soltesz I (2002). Mossy cells in epilepsy: rigor mortis or vigor mortis? *Trends Neurosci* **25**, 140–144.

Ribak CE, Seress L & Amaral DG (1985). The development, ultrastructure and synaptic connections of the mossy cells of the dentate gyrus. *J Neurocytol* **14**, 835–857.

Ruiz A, Fabian-Fine R, Scott R, Walker MC, Rusakov DA & Kullmann DM (2003). GABAA receptors at hippocampal mossy fibers. *Neuron* **39**, 961–973.

Santhakumar V, Bender R, Frotscher M, Ross ST, Hollrigel GS, Toth Z & Soltesz I (2000). Granule cell hyperexcitability in the early post-traumatic rat dentate gyrus: the 'irritable mossy cell' hypothesis. *J Physiol* **524**, 117–134.

Scharfman HE (1992). Blockade of excitation reveals inhibition of dentate spiny hilar neurons recorded in rat hippocampal slices. *J Neurophysiol* **68**, 978–984.

Scharfman HE (1994). Evidence from simultaneous intracellular recordings in rat hippocampal slices that area CA3 pyramidal cells innervate dentate hilar mossy cells. *J Neurophysiol* **72**, 2167–2180.

Scharfman HE (1995). Electrophysiological evidence that dentate hilar mossy cells are excitatory and innervate both granule cells and interneurons. *J Neurophysiol* **74**, 179–194.

Scharfman HE, Kunkel DD & Schwartzkroin PA (1990). Synaptic connections of dentate granule cells and hilar neurons: results of paired intracellular recordings and intracellular horseradish peroxidase injections. *Neuroscience* **37**, 693–707.

Scharfman HE & Schwartzkroin PA (1988). Electrophysiology of morphologically identified mossy cells of the dentate hilus recorded in guinea pig hippocampal slices. *J Neurosci* **8**, 3812–3821.

Soltesz I, Bourassa J & Deschenes M (1993). The behavior of mossy cells of the rat dentate gyrus during theta oscillations in vivo. *Neuroscience* **57**, 555–564.

Soriano E & Frotscher M (1994). Mossy cells of the rat fascia dentata are glutamate-immunoreactive. *Hippocampus* **4**, 65–69.

Stuart G (1999). Voltage-activated sodium channels amplify inhibition in neocortical pyramidal neurons. *Nat Neurosci* **2**, 144–150.

Szabadics J, Varga C, Molnar G, Olah S, Barzo P & Tamas G (2006). Excitatory effect of GABAergic axo-axonic cells in cortical microcircuits. *Science* **311**, 233–235.

Tamas G & Szabadics J (2004). Summation of unitary IPSPs elicited by identified axo-axonic interneurons. *Cereb Cortex* **14**, 823–826.

Thomas AM, Corona-Morales AA, Ferraguti F & Capogna M (2005). Sprouting of mossy fibers and presynaptic inhibition by group II metabotropic glutamate receptors in pilocarpine-treated rat hippocampal slice cultures. *Neuroscience* **131**, 303–320.

Vervaeke K, Hu H, Graham LJ & Storm JF (2006). Contrasting effects of persistent Na^+ current on neuronal excitability and spike timing. *Neuron* **49**, 257–270.

Vida I, Bartos M & Jonas P (2006). Shunting inhibition improves robustness of gamma oscillations in hippocampal interneuron networks by homogenising firing rates. *Neuron* **49**, 107–117.

Wenzel HJ, Buckmaster PS, Anderson NL, Wenzel ME & Schwartzkroin PA (1997). Ultrastructural localization of neurotransmitter immunoreactivity in mossy cell axons and their synaptic targets in the rat dentate gyrus. *Hippocampus* **7**, 559–570.

Williams SR & Stuart GJ (2003). Voltage- and site-dependent control of the somatic impact of dendritic IPSPs. *J Neurosci* **23**, 7358–7367.

Acknowledgements

This work was supported by the Medical Research Council (UK). We thank Professor Dimitri Kullmann, Professor Peter Jonas, Dr Jozsef Csicsvari, Dr Raffaella Geracitano, David Elfant and Theofanis Karayannis for their comments on a previous version of the manuscript. We wish to thank Professor Peter Jonas for allowing the time and use of his equipment for the measurement of E_{GABA}. We also acknowledge the technical help by Ben Micklem and Romana Hauer. Previous work of Angharad M. Kerr is cited as Thomas A.M.

Author's present address

Angharad M. Kerr: Physiologie I, Herman Herder Str-7, Freiburg, D79104, Germany.